Classification: BIOLOGICAL SCIENCES, Microbiology.

Title: **Polysialic acid is a cellular receptor for human adenovirus 52**

Author affiliation: Annasara Lenman[a,1,2], A. Manuel Liaci[b,1], Yan Liu[c], Lars Frängsmyr[a], Martin Frank[d], Bärbel S. Blaum[b], Wengang Chai[c], Iva I. Podgorski[e,f], Balázs Harrach[e], Mária Benkő[e], Ten Feizi[c], Thilo Stehle [b,g,2] and Niklas Arnberg[a]

[a]Division of Virology, Department of Clinical Microbiology, and Laboratory for Molecular Infection Medicine Sweden, Umeå University, SE-90185 Umeå, Sweden, [b]Interfaculty Institute of Biochemistry, University of Tübingen, D-72076 Tübingen, Germany, [c]Glycosciences Laboratory, Department of Medicine, Imperial College London, W12 0NN, UK, [d]Biognos AB, PO Box 8963, SE-40274 Gothenburg, Sweden, [e]Institute for Veterinary Medical Research, Centre for Agricultural Research, Hungarian Academy of Sciences, H-1143 Budapest, Hungary, [f]Division of Molecular Medicine, Rudjer Boskovic Institute, 10000 Zagreb, Croatia. [g]Vanderbilt University School of Medicine, Nashville, Tennessee 37232, USA.

[1]These authors contributed equally.

Corresponding author: [2]Correspondence and requests for materials should be addressed to Annasara Lenman (email: annasara.lenman@umu.se, for virology) and to Thilo Stehle (email: thilo.stehle@uni-tuebingen.de, for structural biology).

Keywords: human adenovirus, polysialic acid, short fiber, adenoviral vector, glycan receptor, glycan microarray

ABSTRACT

Human adenovirus 52 (HAdV-52) is one of only three known HAdVs equipped with both a long and a short fiber protein. While the long fiber binds to the coxsackie- and adenovirus receptor, the function of the short fiber in the virus life cycle is poorly understood. Here, we show that the short fiber knob (SFK) specifically recognizes long chains of α-2,8-linked sialic acids (polySia), an unusual posttranslational modification of selected carrier proteins, and that HAdV-52 can use polySia as a receptor on target cells. Structural analyses and structure-guided mutagenesis of the SFK reveal that the non-reducing terminal sialic acid of polySia engages the protein with direct contacts, and that specificity for polySia is achieved through subtle, transient electrostatic interactions with additional sialic acid residues. To the best of our knowledge, this is the first time polySia has been shown to function as a cellular receptor for a human viral pathogen. Our detailed analysis of the determinants of specificity for this interaction has general implications for protein-carbohydrate interactions, particularly concerning highly charged glycan structures, and provides interesting new dimensions on the biology and evolution of species G adenoviruses.

SIGNIFICANCE STATEMENT

We present here that adenovirus type 52 (HAdV-52) attaches to target cells through a mechanism not previously observed by other human pathogenic viruses. The interaction involves unusual, transient, electrostatic interactions between the short fiber capsid protein and polysialic acid (polySia)-containing receptors on target cells. Not much is known about the binding interactions between polySia and natural ligands and our results therefore provide novel insight to not only adenovirus biology but also the structural basis of polySia function. Since polySia can be found in high expression levels in brain and lung cancers where its presence is associated with poor prognosis, we suggest that this polySia-binding adenovirus could be useful for design of vectors for gene therapy of these cancers.

INTRODUCTION

Human adenoviruses (HAdVs) are common human pathogens associated with gastrointestinal, ocular and respiratory infections. To date, 79 different HAdV types have been identified, and they are grouped into seven species (*Human mastadenovirus A* to *G*) (1). HAdVs are non-enveloped viruses whose icosahedral capsid is composed of three major proteins, the fiber, the penton base and the hexon, all of which are known to mediate binding to host cells. The fiber protein, with a terminal knob domain, binds to cellular receptors such as the coxsackie and adenovirus receptor (CAR) (2-4), desmoglein-2 (5), CD46 (6-8) or sialic acid (Sia)-containing glycans (9-11). The penton base interacts with cellular integrins, thereby facilitating endocytosis (12, 13) and endosomal release (14, 15). The hexon protein is the main component of the viral capsid and binds with high affinity to coagulation factors IX and X, resulting in liver tropism through indirect binding to heparan sulfate on hepatocytes (16-18) and, shields the virion from neutralizing antibodies and complement-mediated destruction (19).

HAdV-52 was isolated in 2003 from a small outbreak of gastroenteritis (20). The virus diverged from other HAdVs and was classified into the new species *Human mastadenovirus G* (HAdV-G), which otherwise exclusively contains Old World monkey AdVs. HAdVs are normally equipped with only one fiber protein, but HAdV-52, along with species HAdV-F types HAdV-40 and -41, differ from all other known HAdVs by having two different fiber proteins, one short (coded by gene fiber-1) and one long (fiber-2) (20-22). We showed recently that the knob domain of HAdV-52 long fiber (52LFK) binds to CAR and that the knob domain of the short fiber (52SFK) binds Sia-containing glycoproteins on target cells (23). However, the identity and structure of the cellular Sia-containing glycans have remained unknown.

Sia-containing glycans serve as receptors for a large number of viral pathogens, including influenza A virus, coronavirus, rotavirus, polyomavirus and many others (24). Variations in Sia specificity determine host and tissue tropism, pathogenicity and transmission of multiple viruses. Here we show by employing an extensive glycan microarray analysis that the 52SFK recognizes longer chains of sialic acid residues, known as polysialic acid (polySia), with higher affinity than any other tested glycan. PolySia is a rare posttranslational modification of only nine identified carrier proteins, among them the cell adhesion molecules NCAM (25) and SynCAM-1 (26) as well as Neuropilin-2 (27) and the dendritic cell chemokine receptor CCR7 (28). Polysialylation is most well-known as a modulator of developmental plasticity in the nervous system, but more recently, additional roles in the development of a number of organs such as the liver, kidney, heart, and testes have been unraveled (reviewed in (29)). In the adult brain, polySia expression is drastically downregulated and only retained in few areas that retain plasticity such as the hippocampus, olfactory bulb and hypothalamus (reviewed in (30-32)). However, polySia is not exclusively found in the brain. Newer studies demonstrate additional regulatory roles in innate immune responses (28, 33-36), and in regenerative or anti-inflammatory processes (37-42). Further, polySia is found in high expression levels on several types of cancer including glioma (43-45), neuroblastoma (46, 47), and lung cancer (48, 49). By means of X-ray crystallography, NMR, molecular dynamics simulation and cellular analyses we reveal here a novel function for polySia as a cellular receptor for the short fiber knob of HAdV-52. The 52SFK possesses a unique polySia-binding mode featuring transient polar interactions and electrostatic contributions that extend beyond a fixed anchoring epitope engaging the non-reducing end of the polySia chain. We further provide an evolutionary analysis of the newly found polySia binding pocket within *Human mastadenovirus G*.

RESULTS

HAdV-52 short fiber knob binds to polysialic acid

We showed previously that the binding of HAdV-52 to human epithelial cells is sialic acid-dependent and occurs via the short fiber knob (23). To date, the precise composition and structure of glycans that can be optimally engaged by 52SFK remains unknown. We performed a glycan microarray analysis of 52SFK binding to 128 different sialylated glycans in an attempt to characterize the glycan receptor of HAdV-52. In the array, 52SFK showed relatively weak binding to α-2,3- and α-2,6-linked sialic acids. However, very strong signals were observed for a group of linear α-2,8-linked oligoSia that represent fragments of naturally occurring polySia (Fig. 1 & Table S1). A markedly enhanced binding signal was observed at a degree of polymerization (DP) of 3 or more monosaccharides, with a maximal response at five or more Sia moieties. To confirm the ability of 52SFK to interact with polySia and evaluate the specificity of this interaction, we developed an ELISA with immobilized, *E. coli*-derived polySia (colominic acid; DP≈80-100) and analyzed the attachment of recombinant knob domains from HAdV-52 short fiber, the Sia-binding HAdV-37 fiber (37FK), and the CAR-binding HAdV-5 (5FK) and HAdV-52 long fiber (52LFK). 52SFK bound efficiently to polySia, while the two CAR-binding FKs did not show any binding to this compound (Fig. 2A). 37FK, which binds with relatively high affinity to the branched, disialylated GD1a glycan using a different binding site (11, 23), bound less strongly to polySia than 52SFK. We therefore conclude that HAdV-52 is able to interact preferentially with polySia via the knob domain of its short fiber while having low affinities for a number of monosialylated glycans.

HAdV-52 binds to polysialic acid on human polySia-expressing cells

To test the relevance of polySia recognition by HAdV-52 in a cellular context, we used human polySia-expressing neuroblastoma cells SH-SY5Y, and their polySia-lacking parental cell line SK-N-SH as models for virus binding and infection (50). The levels of polySia on these cells were confirmed by flow cytometry using the anti-polySia antibody mAb735 (Fig. S1). 52SFK bound five times more strongly to polySia-expressing SH-SY5Y cells compared to the control cell line, whereas none of the control knobs, including 37FK, showed a comparable interaction pattern (Fig. 2B). Next, we used monosialic acid-binding lectins to determine the relative levels of glycans with terminal sialic acids on both cell lines to exclude the possibility that the higher 52SFK binding to SH-SY5Y was due to a higher level of glycans with terminal monosialic acids on these cells rather than a specific binding to polySia. In fact, the lectins MAL-I & -II (bind to α-2,3-linked Sia), SNA (binds to α-2,6-linked Sia), and WGA (binds to terminal sialic acid as well as to N-Acetyl-D-glucosamine) all bound better to SK-N-SH cells than to SH-SY5Y cells (Fig. S1), indicating that the parental, polySia-negative SK-N-SH cells have a higher total density of terminal sialic acids. Furthermore, pre-incubation of 52SFK with soluble oligoSia (DP5) reduced 52SFK binding to SH-SY5Y cells with up to 75%, while no effect was observed on 37FK binding (Fig. 2C). Pre-incubating the whole HAdV-52 virions with oligoSia (DP5) also efficiently reduced binding to and infection of SH-SY5Y cells, whereas sialic acid monosaccharide (DP1) did not have as much of an effect (Fig. 3A & C). Neither of the two glycans tested reduced HAdV-5 binding to or infection of SH-SY5Y cells (Fig. 3B & D). Based on these results we conclude that HAdV-52 virions show a clear preference for polySia-expressing cells over cells lacking polySia, that this feature is not shared by sialic acid- or CAR-binding HAdVs, and that the interactions with polySia are mediated by the 52SFK.

PolySia is engaged at the non-reducing end, similarly to mono- and di-sialylated glycans

Using 2-O-methyl-sialic acid as a ligand, we previously identified a sialic acid-binding site on the lateral side of 52SFK (23). This binding site includes a stretch of three adjacent residues that together form a prominent RGN motif (R316-G317-N318). This site is located on a different part of the knob than the binding site of 37FK, which engages sialic acid near its three-fold axis. The features responsible for the increased affinity for polySia are unknown, and it seems possible that additional contacts or an additional epitope that went undetected in earlier studies are formed between 52SFK and polySia. Consequently, we solved the complex crystal structures of 52SFK with three oligoSia glycans (DP3, -4 or -5) as well as the GD3 glycan (Neu5NAcα2,8Neu5NAcα2,3Galβ1,4Glc, representing a disialic acid motif). All complex structures produced similar results, as shown exemplary for DP3 in Fig. 4. Surprisingly, well-defined electron density was only found for a single sialic acid moiety in the canonical binding pocket in all cases. The electron density around O8 and its direction relative to the protein clearly indicate that it is the non-reducing end of the glycan chain that is engaged, and the observed binding mode is identical to the one observed for monosialic acid. In all cases except for GD3, we observed additional electron density for a second sialic acid moiety projecting from the pocket towards the solvent. The overall density for this moiety is weaker, deteriorating from the glycerol group to the pyranose ring and indicating increased flexibility. All structures showed similar angles for the α-2,8-glycosidic linkage (Fig. S2). Interestingly, the second sialic acid moiety does not seem to contribute any directed contacts to the overall interaction, except for a van-der-Waals contact between its N-acetyl group and E328. This contact seems to cause a local decrease of electron density and a slight rotation of the N-acetyl group. The third (and all following) sialic acids could not be unambiguously traced in any of the structures. In order to verify our observations in solution, we employed saturation transfer difference (STD) NMR spectroscopy to screen for glycan

protons of DP3 and DP5 that are placed within 5-6 Å of the protein (shown exemplary for DP3 in Fig. 4B & C). The spectrum of the glycans alone compared well to the literature (51, 52). Since all of the sialic acid repeats were in a highly similar chemical environment in solution, the respective peaks overlap - with the exception of the non-reducing end, which experiences an upfield shift. The experiment showed saturation transfer occurring almost exclusively at the non-reducing end, while the other moieties only received a very moderate spin saturation occurring exclusively in the N-acetyl group region, which is very much consistent with the contacts observed in the crystal structures. In the case of the R316A mutant, which disrupts the canonical RGN motif and prevents 52SFK attachment to sialic acid on A549 cells (23), saturation transfer was completely abrogated. Together, these results demonstrate that 52SFK engages polySia exclusively via its canonical sialic acid binding site, without any additional epitopes present on the protein.

Transient hydrogen bonds and electrostatic effects are major determinants of 52SFK:polySia interactions

A length of more than three sialic acid residues is required for a strong interaction with 52SFK, as seen in our glycan array data (Fig. 1). According to a cell attachment inhibition experiment, which does not underlie the steric constraints of chip-bound probes, a DP of three was sufficient to substantially decrease 52SFK binding at low concentration in solution. A decrease could also be observed with DP2, but only at higher concentrations (Fig. 5A). Similar results were acquired from surface plasmon resonance experiments with immobilized fiber knobs and oligoSia in solution, where the biggest increase in affinity was shown between DP2 and DP3 (Fig. 5B). In combination with the structural data, these findings suggest that effects other than classical directed short-range contacts may account for the increased binding affinity of higher-order polySia compounds of DP3 or more. Given the poly-anionic

character of polySia, we hypothesized that these effects might be caused by electrostatic interactions, which are non-directed and can occur over longer distances than direct interactions such as hydrogen bonds or van-der-Waals contacts. Indeed, an inspection of the electrostatic potential of the 52SFK revealed a positively charged rim located around the sialic acid binding site, which we termed the 'steering rim'. The rim is mainly formed by residues Q320, R321, R316, and K349 (Fig. 6A-D). According to in-solution NMR studies, the poly-anionic polySia seems to at least transiently adopt a left-handed helical conformation (53). However, polySia is expected to be rather flexible in solution due to its linear, non-branched structure and the conformationally less restricted α-2,8-glycosidic linkage (42). In the DP3 complex structure, the second sialic acid moiety is situated above the ε-amino group of K349. We reasoned that if the polySia glycan roughly followed the left-handed helical arrangement proposed by the literature with energy-minimal glycosidic torsion angles similar to those observed between the first two moieties (Fig. S2A-B), the carbohydrate chain would protrude away from the protein surface into the bulk solvent (indicated in Fig. 6E). Since such an arrangement would unlikely be in agreement with an increased affinity for DP3, we performed molecular dynamics simulation of the complex between 52SFK and DP5 on the microsecond timescale in explicit solvent. Throughout this simulation, DP5 shows a flexible structure with dynamic partial helical features (Video S1). Consistent with the results from our STD-NMR experiments, only the non-reducing end is stably associated with the protein (Fig. 7A-B & 6E). However, the simulation shows that the other sialic acid residues transiently approach the protein surface and form favorable contacts with a variety of amino acids, most of which are located in the 'steering rim' and the closely adjacent R347 (Fig. 7A-D). While the sialic acid moieties adjacent to the non-reducing end mainly interact with a subset of residues located in the canonical pocket and 'steering rim', the moieties towards the reducing end show a much more variable interaction pattern with low occupancies for

individual contacts. In total however, the large majority of contacts are being formed with the canonical pocket or 'steering rim', respectively. The dimensions of DP5 are similar to the combined radius of the binding pocket and 'steering rim' (Fig. 7A-B). In particular, the fifth sialic acid engages in a large number of low-intensity interactions with residues outside the rim according to our simulations (Fig. 7 C-D), which might explain why the enhancing effect of additional Sia moieties is fading beyond DP5 (Fig. 1) and why colominic acid is only moderately more potent than DP5 given the size difference (Fig. 5B). Over the time course of the simulation, the sialic acids display an alternating pattern of transient interactions, and there are most of the time at least two pyranoses that directly interact with the protein (Fig. 7E). This avidity effect is only possible if there are at least three Sia moieties. The average number of favorable interactions found in the canonical pocket and the 'steering rim' per residue are shown in Fig. 7F. Overall, the data agree remarkably well with the other experiments and strongly suggest that transient contact interactions of the third to fifth sialic acid moiety are responsible for the increased binding affinity, while the non-reducing sialic acid is a necessary feature and engaged in a shape-complementary binding site. The involvement of additional non-contact electrostatic interactions could further contribute to binding affinity, as suggested by the opposite charges between the polySia chain and the 'steering rim'.

To provide additional experimental support for this hypothesis, we produced fiber knobs with mutations in the 'steering rim', and analyzed knob binding to polySia-expressing SH-SY5Y cells. The K349A mutant almost completely lost its cell binding capacity, and similar effects were observed for the R321Q and analogous mutants (Fig**.** 7G). When mutated, residue R321 can no longer counterbalance the charge of the proximal side chain of E348, which then likely repelled the polyanionic polySia and might thus contribute to an unexpectedly strong loss in

binding. Indeed, if E348 is also mutated to a non-charged residue, the effect of the R321Q mutation is largely reversed (Fig. 7G). This implies that R321 interacts more weakly with polySia than R316 and K349 do, which fits well with the assumption of a flexible 'pseudo-helical' arrangement.

The polySia binding site and the 'steering rim' are conserved in closely related simian adenoviruses

The polySia-binding RGN motif is conserved in the short fibers of other closely related members of species HAdV-G: SAdV-1, -2, -7 and -11, as well as SAdV-19 (SAdV-C, which obtained its short fiber from an unknown type/species) (54), but it is not found in any other known non-human or human AdV, including the short fiber knobs of HAdV-40 and -41 (HAdV-F) (Fig. S3A). Interestingly, the three positively charged residues forming the 'steering rim' are also functionally conserved in these SAdV types, but in different permutations (RRK, RKK, RRR) (Fig. S3A). Another functionally important residue is Q320, which aids in the production of an electropositive field in the 'steering rim' and is functionally conserved in all of the SAdV types of HAdV-G (but not in SAdV-19). No other HAdV fiber knob with known structures exhibits a comparable 'steering rim' (Fig. S3B). In fact, the lateral part of the knob is typically used for protein interfaces, e.g. for CAR or CD46 (55). However, since the two fibers of HAdV-52 display a clear division of labor, the 52SFK likely serves as a purely Sia-binding fiber knob and thus can accommodate Sia-containing glycans at a more prominently exposed lateral binding site than e.g. HAdV-37. In the HAdV-41 SFK, which is the only other structurally characterized short fiber knob, the disordered G strand is thought to obstruct the electropositive patch on the side (56) making a Sia interaction unlikely. HAdV-5 possesses an electropositive patch, but lacks a shape-complementary Sia-binding site and has never been reported to use sialic acid as attachment receptor. Instead, it has been used as a negative control

in many studies (Fig. 2 & 3). This further supports our hypothesis that polySia binding is a specific ability limited to a small subset of AdVs. We assayed the polySia specificity and binding capacity of fiber knobs belonging to this subset in a cell attachment assay with cells expressing or lacking polySia. All of the examined short knobs except that of SAdV-2 SFK bound better to polySia-expressing cells than the control cell line (Fig. 8). One possible explanation for the inability of SAdV-2 SFK to bind polySia, despite a conserved 'steering rim', could be that this knob harbors a sequence more distantly related to the other knobs (Fig. S3C), which might result in a different overall arrangement of the residues. Nonetheless, 52SFK still displayed the strongest discrepancy between SH-SY5Y and SK-N-SH cells, indicating a more specific interaction of 52SFK with polySia rather than a general high binding to both cell lines as seen for SAdV-7SFK (Fig. 8).

DISCUSSION

We show here that HAdV-52 specifically engages cell surface-expressed polySia via its SFK, employing direct protein-carbohydrate contacts as well as longer-range electrostatic steering forces. As to the best of our knowledge, this is the first time polySia is shown to function as a cellular receptor for a human pathogenic virus. Although a growing number of polySia-binding proteins has been identified (57-63), there are few in-depth structural analyses on the determinants of specificity for polySia, and so far no other polySia-binding protein has been reported to use the unusual binding mode presented here. We therefore believe that our analysis provides a useful framework for a better understanding of general aspects of the interactions of polySia with its binding partners and it remains to be seen whether polySia reacts with its other binding partners similar to that predicted for human adenovirus.

PolySia was identified as a potential receptor for 52SFK in our glycan microarray screen (Fig. 1). In that same array, 52SFK also showed weaker binding to a number of glycans with single capping α-2,3-linked sialic acids, which we also observed in our previous study using a smaller array (23). In a cellular context however, blocking or removing α-2,3-linked sialic acids from the cell surface only had a minor effect on HAdV-52 attachment (23). In comparison, polySia is a more effective ligand. The polySia binding site of HAdV-52 accomplishes the challenging task of maintaining a large pool of ligands while developing increased affinity for a specific subset of surface molecules using just a single binding site. 52SFK can engage α-2,3 and α-2,8 linked sialylated glycans, which bind with their terminal, non-reducing sialic acid moieties to the same epitope using identical direct contacts. The much higher specificity for α-2,8 linked compounds, including polySia, is generated through a multitude of transient contacts between residues surrounding the binding site and sialic acid residues that are distal to the non-reducing end of the polySia chain. These transient contacts

ensure that most of the time at least two Sia moieties are simultaneously associated with the protein, providing an avidity effect. In this manner, mono- and disialylated glycans are still able to interact with the knob with lower affinities, but long-range electrostatic and transient polar interactions enable higher-affinity binding of oligosialic acids with a higher degree of polymerization (DP≥3). In a physiological context, this might reflect the ability of HAdV-52 to adapt to different surface glycan landscapes presented by different cells, hosts, or even commensal bacteria. In humans, it is unknown in which contexts HAdV-52 might encounter polySia for cell attachment. The two most efficient attachment factors of HAdV-52, polySia and CAR, have different expression profiles in the human body and are recognized by the two separate HAdV-52 fiber proteins. In light of its limited genome size, the virus likely draws an evolutionary advantage from being able to interact with two attachment factors. The close evolutionary relationship between HAdV-52 and simian AdVs, and the polySia-binding capacity of these AdVs (Fig. 8), also indicate that polySia might play a role as a cellular attachment factor for viruses that infect other mammals. Sialic acid-containing glycans are known to serve as attachment factors for a number of animal AdVs such as turkey and canine AdV (64, 65). The observed interaction between HAdV-52 and polySia therefore provides an interesting new angle to the known rules that govern virus:glycan receptor interactions, which may be translated to other glycan-binding pathogens.

PolySia can be found in high expression levels on many tumors and its expression is frequently associated with high tumor aggressiveness and invasiveness, resulting in poor clinical prognosis (43, 66, 67). Cancers expressing polySia are also often recurrent and non-responsive to conventional treatments (43), and therefore attention has been drawn to novel therapeutic approaches, including AdV vectors for gene delivery and the use of modified oncolytic AdVs. In a recent approach, the fiber knob of HAdV-5 was substituted with

endosialidaseNF, a tail spike protein from the bacteriophage K1F to generate an efficient polySia-targeting oncolytic vector (68). HAdV-52, a naturally-occurring, unmodified HAdV that already binds polySia, could form the basis for a viable alternative strategy for developing oncolytic vectors, especially in light of its low seroprevalence rates and reduced liver tropism (23, 69). The specificity for polySia can also be increased further by mutating K349 to an arginine (Fig. 7G). With this is mind, we suggest that HAdV-52 based vectors could have a potential for treatment of cancers characterized by elevated polySia-expression.

MATERIALS AND METHODS

Cells and viruses

Human neuroblastoma SK-N-SH cells (purchased from LGC Promochem) were grown in Dulbecco´s modified Eagle medium (DMEM) supplemented with 10% FBS, 20 mM HEPES, 20 U/ml penicillin, 20 µg/ml streptomycin. Human neuroblastoma SH-SY5Y cells (LGC Promochem) were grown in DMEM:Ham´s-F12 (Sigma-Aldrich) 1:1, with the same supplements as the parental SK-N-SH cell line. HAdV-52 (HAdV-G, strain TB3-2243) (20) and HAdV-5 (HAdV-C, strain Ad75; source ATCC) virions were produced with or without ^{35}S-labeling in A549 cells as described previously (70), with the exception that the virions were eluted in sterile phosphate buffered saline (PBS) when desalting on a NAP column (GE Healthcare).

Production of fiber knobs for cell-based assays and ELISA

52SFK and 52LFK were produced as described previously (23). HAdV-37 FK (amino acids 172-365) and HAdV-5 FK (387-581) were produced in the same manner. Simian adenovirus 1 (SAdV-1, HAdV-G) SFK (183-363), SAdV-2 (HAdV-G) SFK (132-312), SAdV-7 (HAdV-G) SFK (167-347), SAdV-11 (HAdV-G) SFK (183-364) and SAdV-19 (*Simian mastadenovirus C*) SFK (101-286) were all cloned with the same RGS-hexa-histidine tag as the fiber knobs described above. SAdV fiber knobs were expressed in *E. coli* (strain Rosetta) and purified with Ni-NTA agarose beads followed by anion exchange (Q-Sepharose). Fiber knob mutants of 52SFK were generated using a QuikChange mutagenesis kit (Agilent Technologies). The following mutants were produced: 1) K349A, 2) R321Q, 3) R321Q/E348Q, 4) R321I, 5) R321V, 6) R321L, 7) K349A/R321Q and 8) K349R. All mutants were produced as 52SFK, described above, and all fiber knobs were analysed by denaturing

gel electrophoresis (NuPAGE Bis-Tris, LifeTechnologies) and Western blots with monoclonal antibodies directed against the His-tag (Qiagen).

Glycan microarray

Microarray analyses were carried out using the neoglycolipid (NGL)-based microarray system (71). Details of the glycan probe library, the generation of the microarrays, imaging and data analysis are in Supplementary Glycan Microarray Document (Table S2) in accordance with the MIRAGE (Minimum Information Required for A Glycomics Experiment) guidelines for reporting glycan microarray-based data (72). In brief, the microarrays were composed of lipid-linked oligosaccharide probes robotically printed at 2 and 5 fmol per spot in duplicate. The microarray binding assay of the recombinant His-tagged 52SFK was performed at 20°C, essentially as described previously (73). In brief, the arrayed slide was blocked for 1 h with 5 mM HEPES pH 7.4, 150 mM NaCl, 5 mM $CaCl_2$, 0.3% (v/v) Blocker Casein (Pierce), 0.3% (w/v) bovine serum albumin (Sigma) (0.3% casein/0.3% BSA). 52SFK was pre-complexed with mouse monoclonal anti-poly-histidine (Ab1) and biotinylated anti-mouse IgG antibodies (Ab2) (both from Sigma) in a ratio of 4:2:1 (by weight). The 52SFK-antibody pre-complexes were prepared by pre-incubating Ab1 with Ab2 for 15 min at ambient temperature, followed by addition of 52SFK and incubation for an additional 15 min on ice. The VP1-antibody complexes were diluted in 0.3% casein/0.3% BSA, to give a final 52SFK concentration of 150 µg/ml, and overlaid onto the arrays at 20°C for 2 h. Binding was detected with Alexa Fluor-647-labelled streptavidin (Molecular Probes). Binding signals were probe-dose dependent. The results of 128 glycan probes at 5 fmol per spot are presented as histogram chart (Fig. 1) and table (Table S1) which includes the list glycan probes present in the array (in house designation ‘Sialyl Glycan Array Sets 40,41’),

binding intensities and errors (difference of signal intensities of duplicate spots of each glycan probe).

ELISA

Ninetysix-well plates (Nunc MaxiSorp, Thermo Scientific) were coated with 1 µg/ml of colominic acid (Sigma-Aldrich) for 2 h at room temperature (RT) in coating buffer (100 mM bicarbonate/carbonate, pH 9.6). The plate was blocked with asialofetuin type II (Sigma-Aldrich) 1 mg/ml in PBS-T (phosphate-buffered saline, 140 mM NaCl, 2.7 mM KCl, 10 mM phosphate buffer pH 7.4, supplemented with 0.05% Tween-20) for 1 h at RT and then washed three times with PBS-T. Meanwhile, fiber knobs (10 µg/ml) were incubated with monoclonal anti RGS-His antibodies (Qiagen; dilution 1:1000 in PBS-T) for 1 h at RT. The wells were then washed three times with PBS-T and incubated with fiber knob:antibody mixtures for 1 h at RT. After washing, the plate was incubated with a HRP-conjugated rabbit anti-mouse IgG antibody (Dako Cytomation; diluted 1:2000 in PBS-T) for 1 h at RT. The wells were washed again and incubated with 100 µl enhanced K-Blue TMB substrate (Neogen Europe) for 15 min and the reaction was then stopped by addition of 100 µl 1 M H_2SO_4. The absorbance was measured at 450 nm using Tecan infinite F2000 Pro (Tecan Nordic AB).

Flow cytometry

Cells were detached with PBS-EDTA (PBS supplemented with 0.05% EDTA), reactivated in growth medium for 1h at 37˚C, pelleted in 96-well plates ($2x10^5$ cells/well) and washed once with binding buffer (BB: DMEM supplemented with 20 mM HEPES, 20 U/ml penicillin + 20 µg/ml streptomycin and 1% BSA). Fiber knobs were added (10 µg/ml in BB) to the cells and incubated for 1 h on ice. Unbound fiber knobs were washed away with PF buffer (PBS supplemented with 2% FBS) and the cells were then incubated with an anti RGS-His mouse

monoclonal antibody (Qiagen; diluted 1:200 in PF) for 30 min. Followed by one wash with PF, the cells were incubated with an Alexa Fluor 488-conjugated secondary antibody (Life Technologies, donkey-anti mouse A488, dilution 1:1000 in PF) for 30 min on ice. Thereafter the cells were washed once with PF and analysed with flow cytometry using FACSLSRII instrument (Becton Dickinson). Results were analysed using FACSDiva software (Becton Dickinson).

The experiment was performed with the following variations: i) fiber knobs were pre-incubated with different concentrations of [α-2,8]-linked oligoSia (N-acetyl neuraminic acid DP2-5, Gerbu/Nakalai) for 1 h on ice before addition to cells; ii) cells were incubated on ice for 30 min with 4 µg/ml of biotinylated a) *M. amurensis* type I or II (MAL I or II) lectins, b) *S. nigra* (SNA) lectins, c) wheat germ agglutinin (WGA; all from Vector Laboratories), or d) monoclonal mouse-anti polySia antibody (mab735, kind gift from Rita Gerardy-Schahn, 1:500) diluted in PF-buffer. Following a-c, the cells were incubated for 30 min on ice with a 1:100 diluted streptavidin-FITC for MAL I & II, SNA and WGA, or (following d), incubated for 30 min on ice with an Alexa Fluor 488-conjugated secondary antibody (donkey-anti mouse A488, dilution 1:1000 in PBS).

Virion binding experiments

Cells were detached with PBS-EDTA, reactivated in growth medium for 1 h at 37˚C (in solution), pelleted in 96 well plates ($2x10^5$ cells/well) and washed with BB. Meanwhile ^{35}S-labeled virions ($0.5x10^9$ virions) were preincubated with different concentrations of [α-2,8]-linked oligoSia diluted in BB for 1 h on ice. 50 µl/well of virion:oligoSia mixtures were then added to cells and incubated for an additional 1 h on ice. Unbound virions were washed away with BB and the cell associated radioactivity was measured in a Wallac 1409 liquid scintillation counter (Perkin-Elmer).

Infection experiments

HAdV-52 and HAdV-5 virions were preincubated with different concentrations of [α-2,8]-linked oligoSia diluted in DMEM supplemented with 20 mM HEPES, 20 U/ml penicillin and 20 µg/ml streptomycin for 1 h on ice. Meanwhile SH-SY5Y cells, grown as a monolayer in black 96-well plate with transparent bottom, were washed three times with serum-free medium. 50 µl/well of virion:oligoSia mixtures were then added to the cells and incubated for an additional 1 h on ice. After incubation, the wells were washed three times with serum-free medium in order to remove unbound virions. Cell culture medium containing 2% FBS was added and the plate was incubated at 37˚C. After 44 h the cells were washed once with PBS, fixed with methanol and stained for AdV hexon (Millipore, mab8052, diluted 1:200 in PBS) for 30 min at RT. After washing twice with PBS an Alexa Fluor 488-conjugated secondary antibody (Life Technologies, donkey-anti mouse A488, dilution 1:1000 in PBS) was added and incubated for 30 min at RT. Following two washes the stained plates were imaged using a Trophos system (Luminy Biotech Enterprises).

Saturation transfer difference NMR

NMR spectra were recorded at 285 K using 3 mm tubes (200 µL sample volume) and a Bruker AVIII-600 spectrometer equipped with a room temperature probe head and processed with TOPSPIN 3.0 (Bruker). Samples contained 1 mM of [α-2,8]-linked oligoSia (DP3 or DP5) and 20 µM of 52SFK WT or R316A mutant protein (monomeric concentration). The proteins were buffer-exchanged prior to NMR experiments to 20 mM potassium phosphate pH 7.4, 150 mM NaCl in D_2O and the glycans were subsequently added from concentrated stock solutions in D_2O. Off- and on-resonance irradiation frequencies were set to -30.0 ppm and 7.0 ppm, respectively. The irradiation power of the selective pulses was 57 Hz, the saturation time was 2 s, and the total relaxation delay was 3 s. A 50 ms continuous-wave spin-lock pulse

with a strength of 3.2 kHz was employed to suppress residual protein signals. A total number of 512 scans and 10,000 points were collected, and spectra were multiplied with a Gaussian window function prior to Fourier transformation.

Crystallization, data collection, and refinement of complex structures

Crystals of 52SFK were prepared as described previously (23). PolySia complex crystals were generated by soaking in 17.5% (w/v) PEG 1000, 12.5% (v/v) PEG 3350, 12.5% MPD, 100 mM Bicine/Tris pH 8.5 supplemented with 50 mM [α-2,8]-linked oligoSia (DP3, -4, or -5) for 18 to 36 h. The GD3 complex structure was prepared by soaking with 20 mM GD3 (Elicityl) for 1.5 h. No cryoprotection was necessary for crystal freezing. Data collection was done at the X06DA beamline of the Swiss Light Source (Villigen) at a wavelength of 1 or 0.92 Å using a Pilatus 2M detector. Structures were indexed with XDS (74) and initial phases were obtained by molecular replacement with Molrep (75) using a published 52SFK structure (PDB-ID: 4XL8) as a template. The structures were refined using phenix.refine (76) and Refmac5 (77) from the PHENIX and CCP4 software suites, respectively, using threefold NCS restraints. Figures were prepared with PyMOL (The PyMOL Molecular Graphics System, Version 1.8, Schrödinger, LLC). Data collection and refinement statistics can be found in Tables S3 and S4. Poisson-Boltzmann electrostatic distributions were calculated using the PDB2PQR and APBS plugins in PyMOL (78, 79).

Surface plasmon resonance

52SFK was diluted in running buffer (HBS-EP+; GE Healthcare) to a concentration of around 0.03 μM (0.022-0.035 μM) and captured on the Ni-NTA sensor chip (GE Healthcare) according to the manufacturer's instructions, resulting in an immobilization density between 700-900 RU. In short: an automated program cycle of the following sequence: (1) activation

of the sensor chip with Ni (II), (2) capture of 52SFK, (3) analyte injection, (4) regeneration of the surface with 0.35 M EDTA, and (5) rinse with HBS-EP+ without EDTA. All steps were performed at a flow rate of 30 µl/min. All binding assays were carried out at 25°C, and HBS-EP+ buffer was used as running buffer. The analytes ([α-2,8]-linked oligoSia DP3, -4, -5 and colominic acid) were serially diluted in running buffer to prepare a two-fold concentration series ranging from 0.1 to 8 mM (with small variations depending on the analyte), and then injected in series over the reference and experimental biosensor surfaces for 120 s and a dissociation time of 120 s. Blank samples containing only running buffer were also injected under the same conditions to allow for double referencing.

Molecular dynamics simulation

The complex of 52SFK with three polySia (DP5) glycans was prepared using PDB entry 4XL8 as a starting structure. Two polySia glycans were positioned into their binding sites by superimposing the terminal Neu5Ac residues with the two Neu5Ac residues present in the crystal structure. The remaining polySia glycan was positioned into the third site (unoccupied in 4XL8) by taking into account the threefold symmetry of 52SFK. The complex was solvated in 0.1% NaCl solution and two independent 1 µs trajectories were sampled at 310 K using YASARA (80). AMBER14 (81) was chosen as the force field, which includes Glycam-06 (82) parameters for carbohydrates. The terminal Neu5Ac residues were kept in their binding site by the application of distance restraints. Snapshots were stored every 25 ps. The interactions of polySia with its 52SFK receptor were analysed based on accumulated 6 µs trajectory data (three polySias, 2 µs each) using Conformational Analysis Tools (www.md-simulations.de/CAT/).

Statistical analysis of cell based assays

ELISA and all cell based experiments were performed three times with duplicate samples in each experiment. The results are expressed as means ± standard deviations and t-test or was performed using GraphPad Prism version 7.00 for Windows, GraphPad Software, San Diego California USA. P-values < 0.05 were considered statistically significant.

ACKNOWLEDGEMENTS

This investigation was supported by grants from the Swedish Cancer Society grant nr. CAN 2015/695, Cancer Research Foundation in Northern Sweden grant nr. AMP 16-794, Knut & Alice Wallenberg foundation grant nr. KAW 2013.0019, the German Research Foundation (DFG-SFB685), the Marie-Curie Initial Training Network "ADVance" FP7-290002, the Glycobiology/Glycobiotechnology program of the Baden-Württemberg Foundation and Welcome Trust grants WT093378MA/Z/10/Z/ and WT099197/Z/12/Z. The neoglycolipid-based glycan microarrays contain several saccharides provided by collaborators whom we thank as well as members of the Glycosciences Laboratory for their collaboration in the establishment of the microarray system.

AUTHOR CONTRIBUTIONS

A.L., A.M.L. and Y.L. designed and carried out experiments, analyzed results, and wrote the manuscript. L.F. and M.F. designed and carried out experiments, analyzed results and reviewed manuscript. B.B., W.C. and I.P. performed experiments. I.P., B.H. and M.B. provided useful ideas and reviewed the manuscript. T.F., T.S. and N.A. designed the study, interpreted results and wrote the manuscript.

REFERENCES

1. Yoshitomi H, Sera N, Gonzalez G, Hanaoka N, & Fujimoto T (2016) First isolation of a new type of human adenovirus (genotype 79), species Human mastadenovirus B (B2) from sewage water in Japan. *J Med Virol*.
2. Bergelson JM, *et al.* (1997) Isolation of a common receptor for Coxsackie B viruses and adenoviruses 2 and 5. *Science* 275(5304):1320-1323.
3. Tomko RP, Xu R, & Philipson L (1997) HCAR and MCAR: the human and mouse cellular receptors for subgroup C adenoviruses and group B coxsackieviruses. *Proc. Natl. Acad. Sci. U S A* 94(7):3352-3356.
4. Roelvink PW, *et al.* (1998) The coxsackievirus-adenovirus receptor protein can function as a cellular attachment protein for adenovirus serotypes from subgroups A, C, D, E, and F. *J Virol.* 72(10):7909-7915.
5. Wang H, *et al.* (2011) Desmoglein 2 is a receptor for adenovirus serotypes 3, 7, 11 and 14. *Nat Med* 17(1):96-104.
6. Gaggar A, Shayakhmetov DM, & Lieber A (2003) CD46 is a cellular receptor for group B adenoviruses. *Nat. Med.* 9:1408-1412.
7. Segerman A, *et al.* (2003) Adenovirus type 11 uses CD46 as a cellular receptor. *J Virol* 77:9183-9191.
8. Marttila M, *et al.* (2005) CD46 is a cellular receptor for all species B adenoviruses except types 3 and 7. *J. Virol.* 79:14429-14436.
9. Arnberg N, Edlund K, Kidd AH, & Wadell G (2000) Adenovirus type 37 uses sialic acid as a cellular receptor. *J Virol* 74:42-48.
10. Arnberg N, Kidd AH, Edlund K, Olfat F, & Wadell G (2000) Initial interactions of subgenus D adenoviruses with A549 cellular receptors: sialic acid versus alpha(v) integrins. *J. Virol.* 74:7691-7693.
11. Nilsson EC, *et al.* (2011) The GD1a glycan is a cellular receptor for adenoviruses causing epidemic keratoconjunctivitis. *Nat Med* 17(1):105-109.
12. Belin MT & Boulanger P (1993) Involvement of cellular adhesion sequences in the attachment of adenovirus to the HeLa cell surface. *J. Gen. Virol.* 74(Pt 8):1485-1497.
13. Wickham TJ, Mathias P, Cheresh DA, & Nemerow GR (1993) Integrins alpha v beta 3 and alpha v beta 5 promote adenovirus internalization but not virus attachment. *Cell* 73(2):309-319.
14. Wickham TJ, Filardo EJ, Cheresh DA, & Nemerow GR (1994) Integrin alpha v beta 5 selectively promotes adenovirus mediated cell membrane permeabilization. *J Cell Biol* 127(1):257-264.
15. Wang K, Guan T, Cheresh DA, & Nemerow GR (2000) Regulation of adenovirus membrane penetration by the cytoplasmic tail of integrin beta5. *J Virol* 74(6):2731-2739.
16. Parker AL, *et al.* (2006) Multiple vitamin K-dependent coagulation zymogens promote adenovirus-mediated gene delivery to hepatocytes. *Blood* 108(8):2554-2561.
17. Waddington SN, *et al.* (2008) Adenovirus serotype 5 hexon mediates liver gene transfer. *Cell* 132(3):397-409.
18. Lenman A, *et al.* (2011) Coagulation factor IX mediates serotype-specific binding of species A adenoviruses to host cells. *J Virol* 85(24):13420-13431.
19. Xu Z, *et al.* (2013) Coagulation factor X shields adenovirus type 5 from attack by natural antibodies and complement. *Nat Med* 19(4):452-457.
20. Jones MS, 2nd, *et al.* (2007) New adenovirus species found in a patient presenting with gastroenteritis. *J Virol* 81(11):5978-5984.

21. Kidd AH, Chroboczek J, Cusack S, & Ruigrok RW (1993) Adenovirus type 40 virions contain two distinct fibers. *Virology* 192(1):73-84.
22. Yeh HY, Pieniazek N, Pieniazek D, Gelderblom H, & Luftig RB (1994) Human adenovirus type 41 contains two fibers. *Virus Res* 33(2):179-198.
23. Lenman A, *et al.* (2015) Human adenovirus 52 uses sialic acid-containing glycoproteins and the coxsackie and adenovirus receptor for binding to target cells. *PLoS Pathog* 11(2):e1004657.
24. Matrosovich M, Herrler G, & Klenk HD (2015) Sialic Acid Receptors of Viruses. *Top Curr Chem* 367:1-28.
25. Finne J, Finne U, Deagostini-Bazin H, & Goridis C (1983) Occurrence of alpha 2-8 linked polysialosyl units in a neural cell adhesion molecule. *Biochem Biophys Res Commun* 112(2):482-487.
26. Galuska SP, *et al.* (2010) Synaptic cell adhesion molecule SynCAM 1 is a target for polysialylation in postnatal mouse brain. *Proc Natl Acad Sci U S A* 107(22):10250-10255.
27. Werneburg S, Muhlenhoff M, Stangel M, & Hildebrandt H (2015) Polysialic acid on SynCAM 1 in NG2 cells and on neuropilin-2 in microglia is confined to intracellular pools that are rapidly depleted upon stimulation. *Glia* 63(7):1240-1255.
28. Kiermaier E, *et al.* (2016) Polysialylation controls dendritic cell trafficking by regulating chemokine recognition. *Science* 351(6269):186-190.
29. Galuska CE, Lutteke T, & Galuska SP (2017) Is Polysialylated NCAM Not Only a Regulator during Brain Development But also during the Formation of Other Organs? *Biology (Basel)* 6(2).
30. Schnaar RL, Gerardy-Schahn R, & Hildebrandt H (2014) Sialic acids in the brain: gangliosides and polysialic acid in nervous system development, stability, disease, and regeneration. *Physiol Rev* 94(2):461-518.
31. Colley KJ, Kitajima K, & Sato C (2014) Polysialic acid: biosynthesis, novel functions and applications. *Crit Rev Biochem Mol Biol* 49(6):498-532.
32. Rutishauser U (2008) Polysialic acid in the plasticity of the developing and adult vertebrate nervous system. *Nat Rev Neurosci* 9(1):26-35.
33. Rey-Gallardo A, *et al.* (2010) Polysialylated neuropilin-2 enhances human dendritic cell migration through the basic C-terminal region of CCL21. *Glycobiology* 20(9):1139-1146.
34. Rey-Gallardo A, Delgado-Martin C, Gerardy-Schahn R, Rodriguez-Fernandez JL, & Vega MA (2011) Polysialic acid is required for neuropilin-2a/b-mediated control of CCL21-driven chemotaxis of mature dendritic cells and for their migration in vivo. *Glycobiology* 21(5):655-662.
35. Curreli S, Arany Z, Gerardy-Schahn R, Mann D, & Stamatos NM (2007) Polysialylated neuropilin-2 is expressed on the surface of human dendritic cells and modulates dendritic cell-T lymphocyte interactions. *J Biol Chem* 282(42):30346-30356.
36. Stamatos NM, *et al.* (2014) Changes in polysialic acid expression on myeloid cells during differentiation and recruitment to sites of inflammation: role in phagocytosis. *Glycobiology* 24(9):864-879.
37. Tsuchiya A, *et al.* (2014) Polysialic acid/neural cell adhesion molecule modulates the formation of ductular reactions in liver injury. *Hepatology* 60(5):1727-1740.
38. El Maarouf A, Petridis AK, & Rutishauser U (2006) Use of polysialic acid in repair of the central nervous system. *Proc Natl Acad Sci U S A* 103(45):16989-16994.
39. Zhang Y, *et al.* (2007) Induced expression of polysialic acid in the spinal cord promotes regeneration of sensory axons. *Mol Cell Neurosci* 35(1):109-119.

40. Zhang Y, *et al.* (2007) Lentiviral-mediated expression of polysialic acid in spinal cord and conditioning lesion promote regeneration of sensory axons into spinal cord. *Mol Ther* 15(10):1796-1804.
41. Werneburg S, *et al.* (2016) Polysialylation and lipopolysaccharide-induced shedding of E-selectin ligand-1 and neuropilin-2 by microglia and THP-1 macrophages. *Glia* 64(8):1314-1330.
42. Ulm C, *et al.* (2013) Soluble polysialylated NCAM: a novel player of the innate immune system in the lung. *Cell Mol Life Sci* 70(19):3695-3708.
43. Suzuki M, *et al.* (2005) Polysialic acid facilitates tumor invasion by glioma cells. *Glycobiology* 15(9):887-894.
44. Petridis AK, Wedderkopp H, Hugo HH, & Maximilian Mehdorn H (2009) Polysialic acid overexpression in malignant astrocytomas. *Acta Neurochir (Wien)* 151(6):601-603; discussion 603-604.
45. Amoureux MC, *et al.* (2010) Polysialic acid neural cell adhesion molecule (PSA-NCAM) is an adverse prognosis factor in glioblastoma, and regulates olig2 expression in glioma cell lines. *BMC Cancer* 10:91.
46. Figarella-Branger DF, Durbec PL, & Rougon GN (1990) Differential spectrum of expression of neural cell adhesion molecule isoforms and L1 adhesion molecules on human neuroectodermal tumors. *Cancer Res* 50(19):6364-6370.
47. Gluer S, Schelp C, Gerardy-Schahn R, & von Schweinitz D (1998) Polysialylated neural cell adhesion molecule as a marker for differential diagnosis in pediatric tumors. *J Pediatr Surg* 33(10):1516-1520.
48. Lantuejoul S, Moro D, Michalides RJ, Brambilla C, & Brambilla E (1998) Neural cell adhesion molecules (NCAM) and NCAM-PSA expression in neuroendocrine lung tumors. *Am J Surg Pathol* 22(10):1267-1276.
49. Tanaka F, *et al.* (2000) Expression of polysialic acid and STX, a human polysialyltransferase, is correlated with tumor progression in non-small cell lung cancer. *Cancer Res* 60(11):3072-3080.
50. Valentiner U, Muhlenhoff M, Lehmann U, Hildebrandt H, & Schumacher U (2011) Expression of the neural cell adhesion molecule and polysialic acid in human neuroblastoma cell lines. *Int J Oncol* 39(2):417-424.
51. Brisson JR, Baumann H, Imberty A, Perez S, & Jennings HJ (1992) Helical epitope of the group B meningococcal alpha(2-8)-linked sialic acid polysaccharide. *Biochemistry* 31(21):4996-5004.
52. Ray GJ, *et al.* (2014) Complete structural elucidation of an oxidized polysialic acid drug intermediate by nuclear magnetic resonance spectroscopy. *Bioconjug Chem* 25(4):665-676.
53. Battistel MD, Shangold M, Trinh L, Shiloach J, & Freedberg DI (2012) Evidence for helical structure in a tetramer of alpha2-8 sialic acid: unveiling a structural antigen. *J Am Chem Soc* 134(26):10717-10720.
54. Podgorski, II, Panto L, Papp T, Harrach B, & Benko M (2016) Genome analysis of four Old World monkey adenoviruses supports the proposed species classification of primate adenoviruses and reveals signs of possible homologous recombination. *J Gen Virol* 97(7):1604-1614.
55. Cupelli K & Stehle T (2011) Viral attachment strategies: the many faces of adenoviruses. *Curr Opin Virol* 1(2):84-91.
56. Seiradake E & Cusack S (2005) Crystal structure of enteric adenovirus serotype 41 short fiber head. *J Virol* 79(22):14088-14094.

57. Kanato Y, Kitajima K, & Sato C (2008) Direct binding of polysialic acid to a brain-derived neurotrophic factor depends on the degree of polymerization. *Glycobiology* 18(12):1044-1053.
58. Sato C, Yamakawa N, & Kitajima K (2010) Measurement of glycan-based interactions by frontal affinity chromatography and surface plasmon resonance. *Methods Enzymol* 478:219-232.
59. Ono S, Hane M, Kitajima K, & Sato C (2012) Novel regulation of fibroblast growth factor 2 (FGF2)-mediated cell growth by polysialic acid. *J Biol Chem* 287(6):3710-3722.
60. Isomura R, Kitajima K, & Sato C (2011) Structural and functional impairments of polysialic acid by a mutated polysialyltransferase found in schizophrenia. *J Biol Chem* 286(24):21535-21545.
61. Mishra B, *et al.* (2010) Functional role of the interaction between polysialic acid and extracellular histone H1. *J Neurosci* 30(37):12400-12413.
62. Nagae M, *et al.* (2013) Crystal structure of anti-polysialic acid antibody single chain Fv fragment complexed with octasialic acid: insight into the binding preference for polysialic acid. *J Biol Chem* 288(47):33784-33796.
63. Haselhorst T, *et al.* (2006) Endosialidase NF appears to bind polySia DP5 in a helical conformation. *Chembiochem* 7(12):1875-1877.
64. Seiradake E, *et al.* (2009) The cell adhesion molecule "CAR" and sialic acid on human erythrocytes influence adenovirus in vivo biodistribution. *PLoS Pathog* 5(1):e1000277.
65. Singh AK, *et al.* (2015) Structure and Sialyllactose Binding of the Carboxy-Terminal Head Domain of the Fibre from a Siadenovirus, Turkey Adenovirus 3. *PLoS One* 10(9):e0139339.
66. Tanaka F, *et al.* (2001) Prognostic significance of polysialic acid expression in resected non-small cell lung cancer. *Cancer Res* 61(4):1666-1670.
67. Falconer RA, Errington RJ, Shnyder SD, Smith PJ, & Patterson LH (2012) Polysialyltransferase: A New Target in Metastatic Cancer. *Current Cancer Drug Targets* 12(8):925-939.
68. Martin NT, *et al.* (2018) Targeting polysialic acid-abundant cancers using oncolytic adenoviruses with fibers fused to active bacteriophage borne endosialidase. *Biomaterials* 158:86-94.
69. Banyai K, *et al.* (2009) Searching for HAdV-52, the putative gastroenteritis-associated human adenovirus serotype in Southern Hungary. *New Microbiol* 32(2):185-188.
70. Johansson SM, *et al.* (2007) Multivalent sialic acid conjugates inhibit adenovirus type 37 from binding to and infecting human corneal epithelial cells. *Antiviral Res.* 73:92-100.
71. Liu Y, *et al.* (2012) Neoglycolipid-based oligosaccharide microarray system: preparation of NGLs and their noncovalent immobilization on nitrocellulose-coated glass slides for microarray analyses. *Methods Mol Biol.* 808:117-136.
72. Liu Y, *et al.* (2016) The minimum information required for a glycomics experiment (MIRAGE) project: improving the standards for reporting glycan microarray-based data. *Glycobiology*.
73. Neu U, *et al.* (2013) Structures of B-Lymphotropic Polyomavirus VP1 in complex with oligosaccharide ligands. *PLoS Pathog.* 9:e1003714.
74. Kabsch W (2010) Xds. *Acta Crystallogr D Biol Crystallogr* 66(Pt 2):125-132.
75. Vagin A & Teplyakov A (1997) MOLREP: an automated program for molecular replacement. *J Appl Crystallogr* 30:1022-1025.

76. Adams PD, *et al.* (2010) PHENIX: a comprehensive Python-based system for macromolecular structure solution. *Acta Crystallogr D* 66:213-221.
77. Murshudov GN, Vagin AA, & Dodson EJ (1997) Refinement of macromolecular structures by the maximum-likelihood method. *Acta Crystallogr D* 53:240-255.
78. Baker NA, Sept D, Joseph S, Holst MJ, & McCammon JA (2001) Electrostatics of nanosystems: Application to microtubules and the ribosome. *P Natl Acad Sci USA* 98(18):10037-10041.
79. Dolinsky TJ, Nielsen JE, McCammon JA, & Baker NA (2004) PDB2PQR: an automated pipeline for the setup of Poisson-Boltzmann electrostatics calculations. *Nucleic Acids Research* 32:W665-W667.
80. Krieger E & Vriend G (2015) New ways to boost molecular dynamics simulations. *J Comput Chem* 36(13):996-1007.
81. Hornak V, *et al.* (2006) Comparison of multiple Amber force fields and development of improved protein backbone parameters. *Proteins* 65(3):712-725.
82. Kirschner KN, *et al.* (2008) GLYCAM06: a generalizable biomolecular force field. Carbohydrates. *J Comput Chem* 29(4):622-655.
83. Vasudevan SV & Balaji PV (2002) Molecular dynamics simulations of alpha2 --> 8-linked disialoside: conformational analysis and implications for binding to proteins. *Biopolymers* 63(3):168-180.

FIGURES

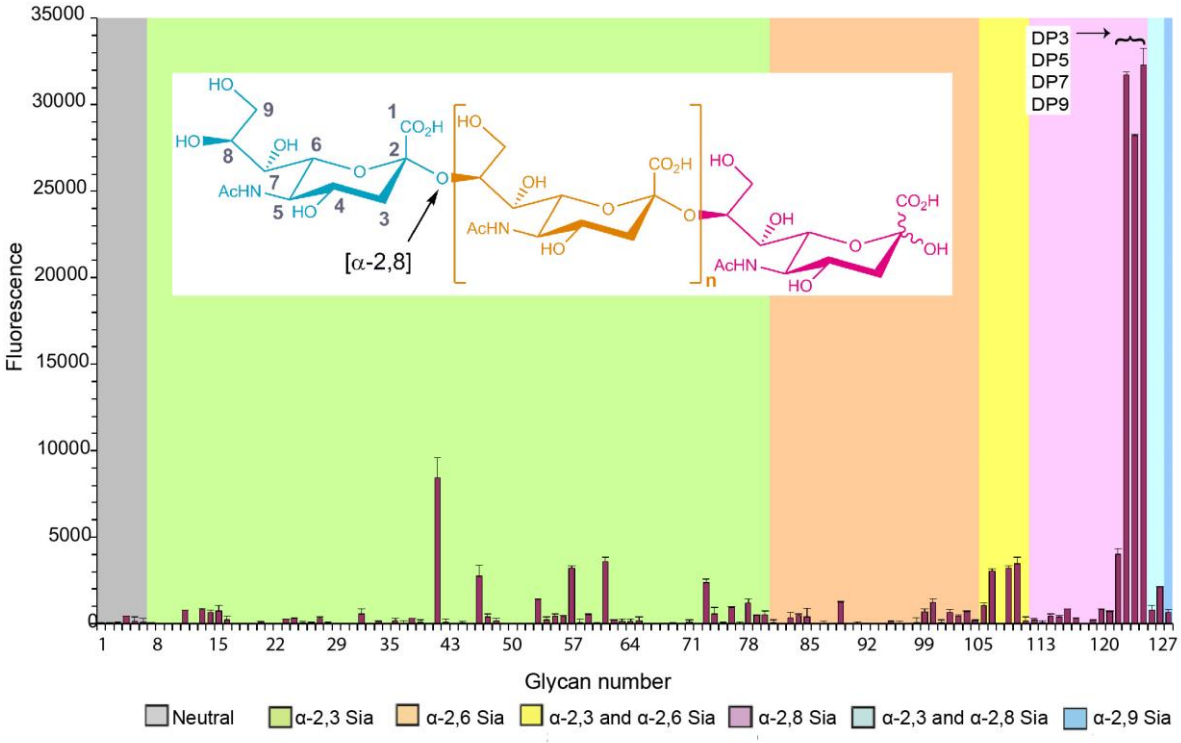

Fig. 1. Glycan array analysis of HAdV-52 short fiber knob interactions with sialylated glycans. The microarray consists of lipid-linked oligosaccharide probes, the sequences are listed in Table S1. The probes are arranged according to terminal sialic acid linkage, oligosaccharide backbone chain length, and sequence. The various types of terminal sialic acid linkages are indicated by the colored panels as defined at the bottom of the figure. Numerical scores for the binding intensity are shown as means of fluorescence intensities of duplicate spots at 5 fmol/spot. Error bars represent half of the difference between the two values. DP3-DP9= [α-2,8]-linked sialic acids with a degree of polymerization (DP) between 3-9 (from left to right, in steps of two). Inlay: general structure of polySia, up to ~100 sialic acid moieties are linearly connected via an [α-2,8]-linkage. Blue: non-reducing end; Pink: reducing end.

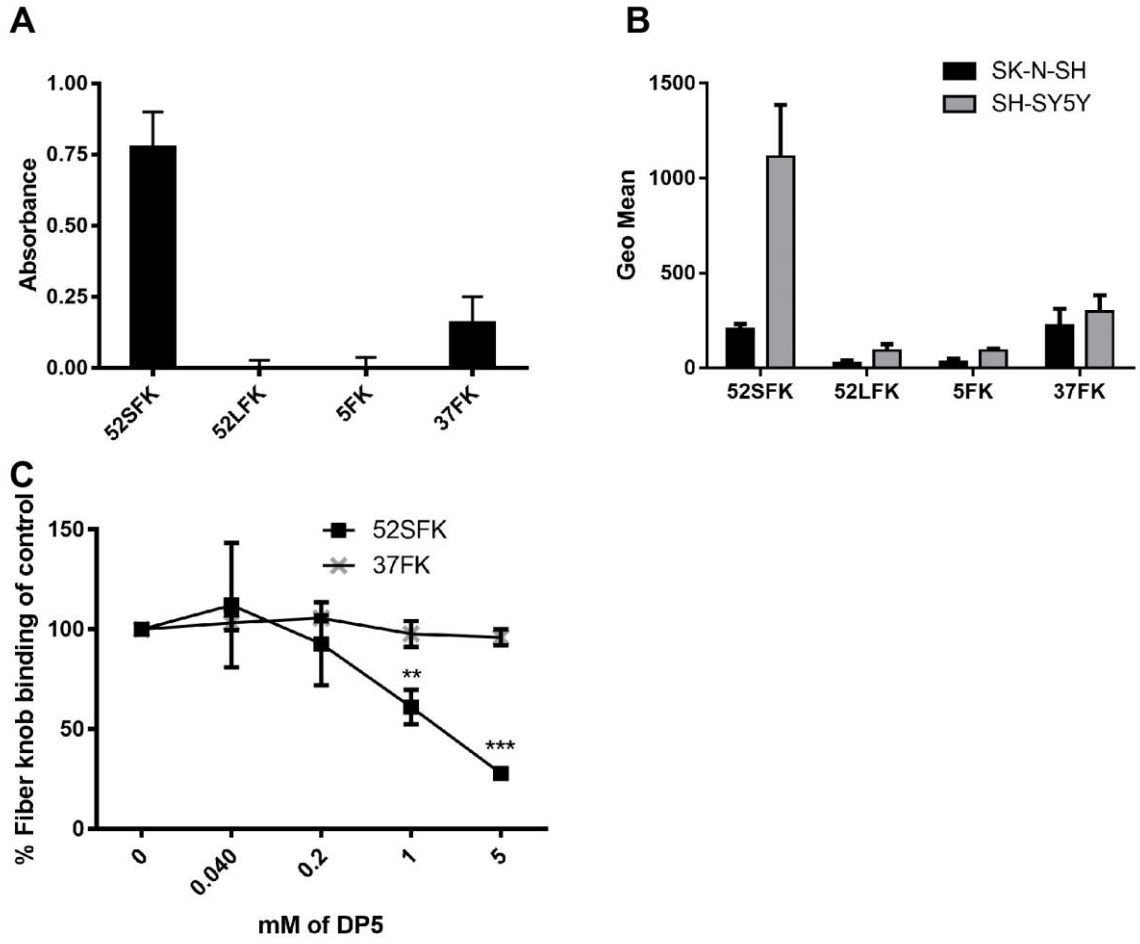

Fig. 2. HAdV-52 short fiber knob binds to polysialic acid. (A) HAdV-fiber knob binding to immobilized E.coli-derived polySia (colominic acid, DP≈80-100). Relative absorbance is shown. (B) Flow cytometry-based quantification of HAdV fiber knob binding to human neuroblastoma cells expressing (SH-SY5Y) or lacking (SK-N-SH) polySia. (C) Flow cytometry-based quantification of 52SFK and 37FK binding to SH-SY5Y cells after fiber knob pre-incubation with increasing concentrations of pentasialic acid (DP5). SFK: short fiber knob; LFK: long fiber knob; FK: fiber knob. All experiments were performed three times with duplicate samples in each experiment. Error bars represent mean ± SD. **indicates $p<0.01$ and *** indicates $p<0.001$.

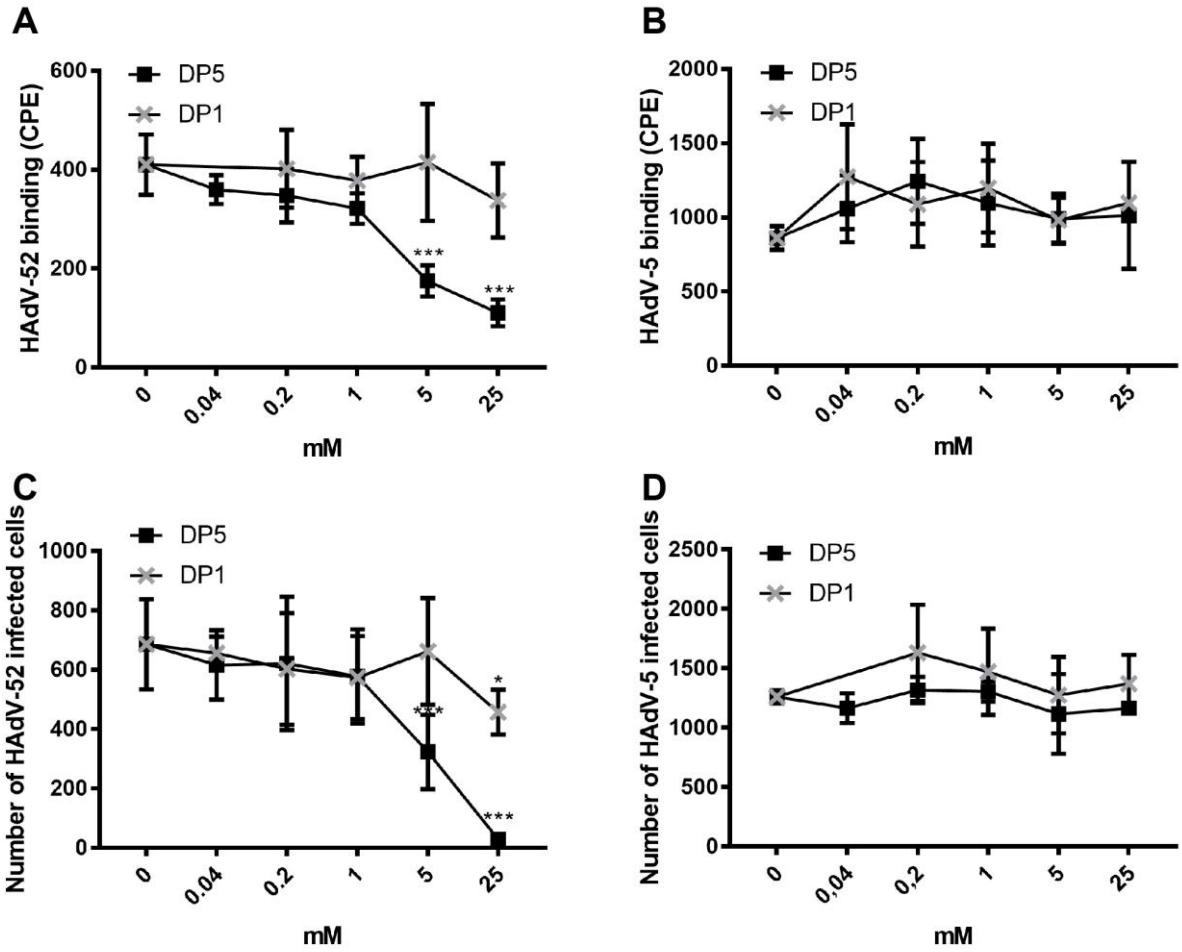

Fig. 3. OligoSia efficiently reduces HAdV-52 virion binding to and infection of SH-SY5Y cells. Binding of (A) ^{35}S-labeled HAdV-52 and (B) ^{35}S-labeled HAdV-5 virions to SH-SY5Y cells after pre-incubation with soluble monosialic acid (DP1) or pentasialic acid (DP5). Infection of SH-SY5Y with (C) HAdV-52 and (D) HAdV-5 after pre-incubation with DP1 or DP5. The experiments were performed three times with duplicate samples in each experiment. Error bars represent mean ± SD. *** indicates $p<0.001$.

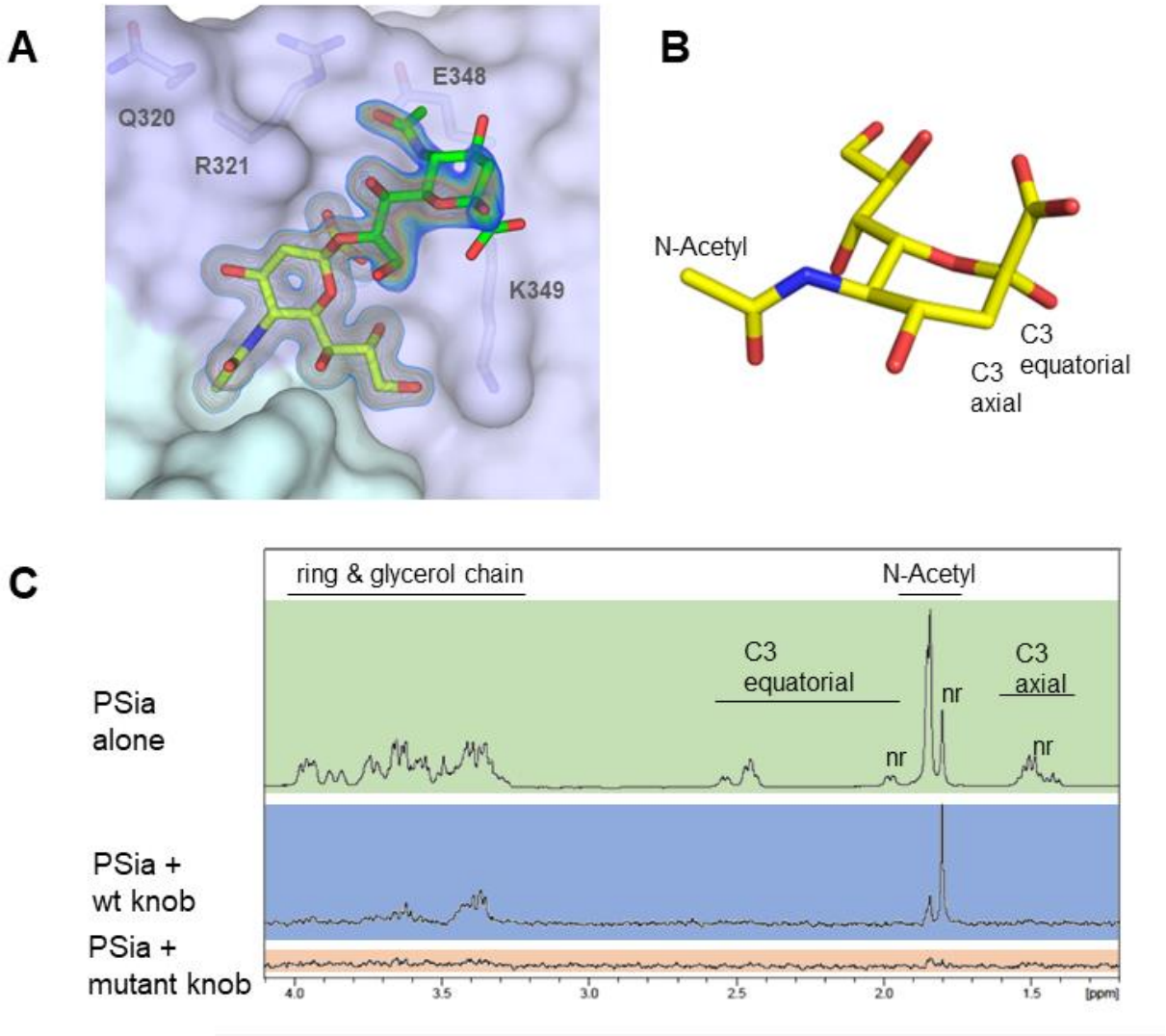

Fig. 4. [α-2,8]-linked oligoSias are engaged in the canonical binding pocket of HAdV-52 short fiber knob via their non-reducing end. (A) Complex structure of 52SFK and trisialic acid (DP3). Shown is a 2Fo-Fc map calculated at 1 σ (blue) and 1.5 σ (orange) after refinement. The non-reducing sialic acid moiety is colored in yellow, the adjacent moiety in green. The third sialic acid moiety could not be resolved. (B) Schematic representation of sialic acid in the α-conformation. The positions of distinctive protons for NMR are indicated. (C) STD-NMR of 52SFK and DP3. Green box: DP3 alone; blue box: Saturation transfer difference spectrum of the 52SFK:DP3 complex; red box: Saturation transfer difference spectrum of the R316A-52SFK:DP3 complex, nr = non-reducing end.

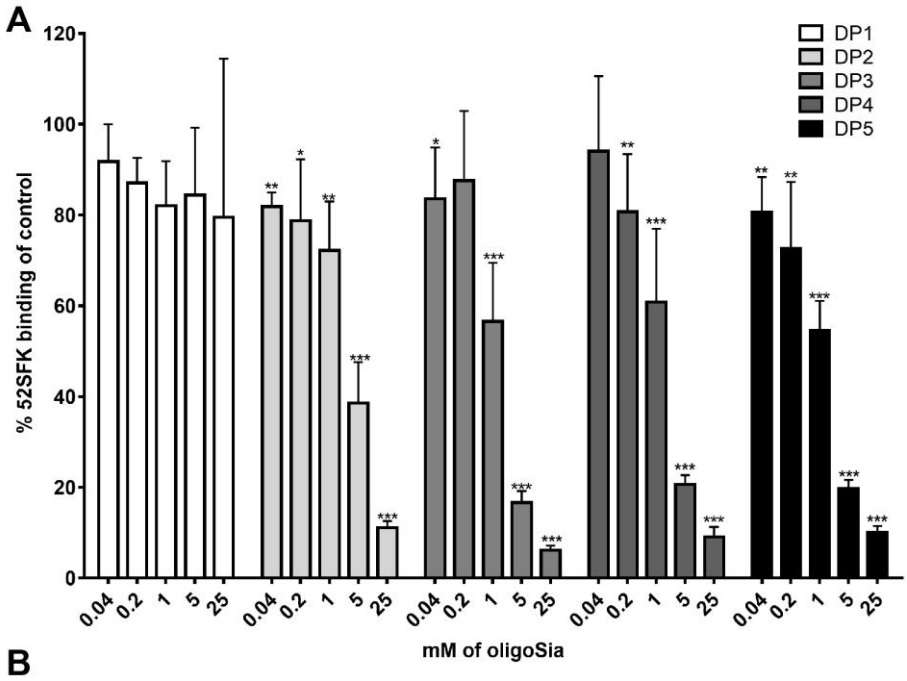

Ligand (immobilized)	Analyte (in solution)	K_D (10^{-3} M)
52SFK	DP2	12.13 ± 0.70
52SFK	DP3	6.60 ± 0.43
52SFK	DP4	6.05 ± 0.21
52SFK	DP5	5.07 ± 0.20
52SFK	*E.coli*-derived PSA	1.11 ± 0.14

Fig. 5. A degree of polymerization of three, or more, strengthens the interactions with 52SFK. (A) Flow cytometry-based quantification of 52SFK binding to SH-SY5Y cells after fiber knob pre-incubation with increasing concentrations of oligoSia. The experiment was performed three times with duplicate samples in each experiment. Error bars represent mean ± SD. *indicates $p<0.05$, **indicates $p<0.01$ and *** indicates $p<0.001$. (B) Surface plasmon resonance analysis of 52SFK binding to disialic acid (DP2), trisialic acid (DP3), tetrasialic acid (DP4), pentasialic acid (DP5) and E. coli-derived polySia (DP≈80-100).

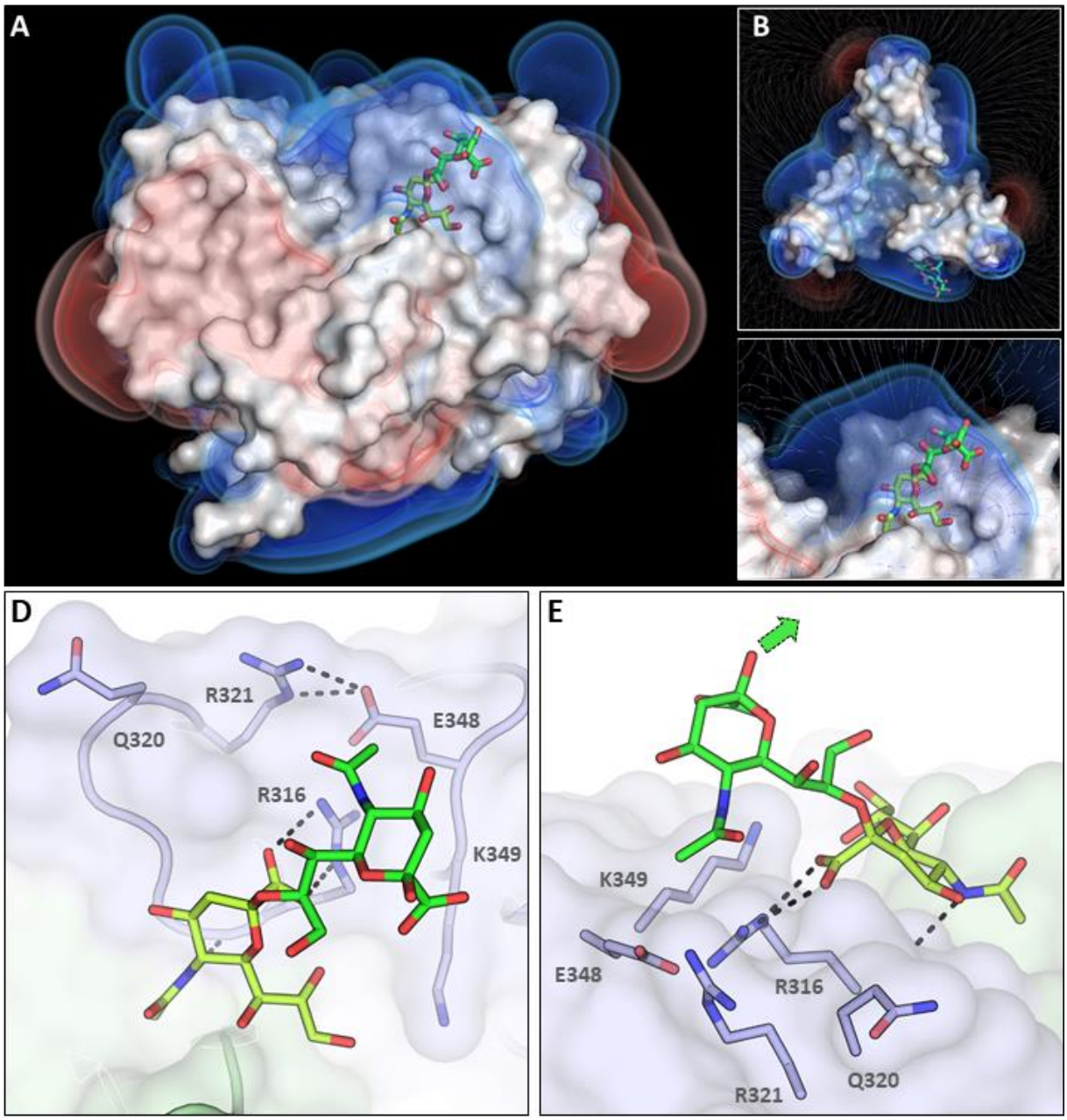

Fig. 6. Representation of the HAdV-52 short fiber knob 'steering rim'. Poisson-Boltzmann electrostatic potential isosurfaces and field lines for the protein were calculated at ±1; ±0.75; ±0.5 kT/e. The positively charged rim can be seen in blue. Bound trisialic acid (DP3) is shown as green sticks. (A) Side view. (B) Top view including field lines. (C) Detailed view of the binding pocket including field lines. (D) Detailed view of the binding pocket showing the relative placement of glycan and 'steering rim' residues. Residues of the 'steering rim' are highlighted as sticks. R321 and E348 are forming a salt bridge, as do R316 and the carboxyl group at the non-reducing end of DP3. The orientation is the same as in Panel A. (E) Side

view of the interaction site. The second sialic acid moiety is projection away from the protein surface. The green arrow indicates the expected direction of the adjacent sialic acid moieties. (D-E) The non-reducing sialic acid moiety is colored in yellow, the adjacent moiety in green.

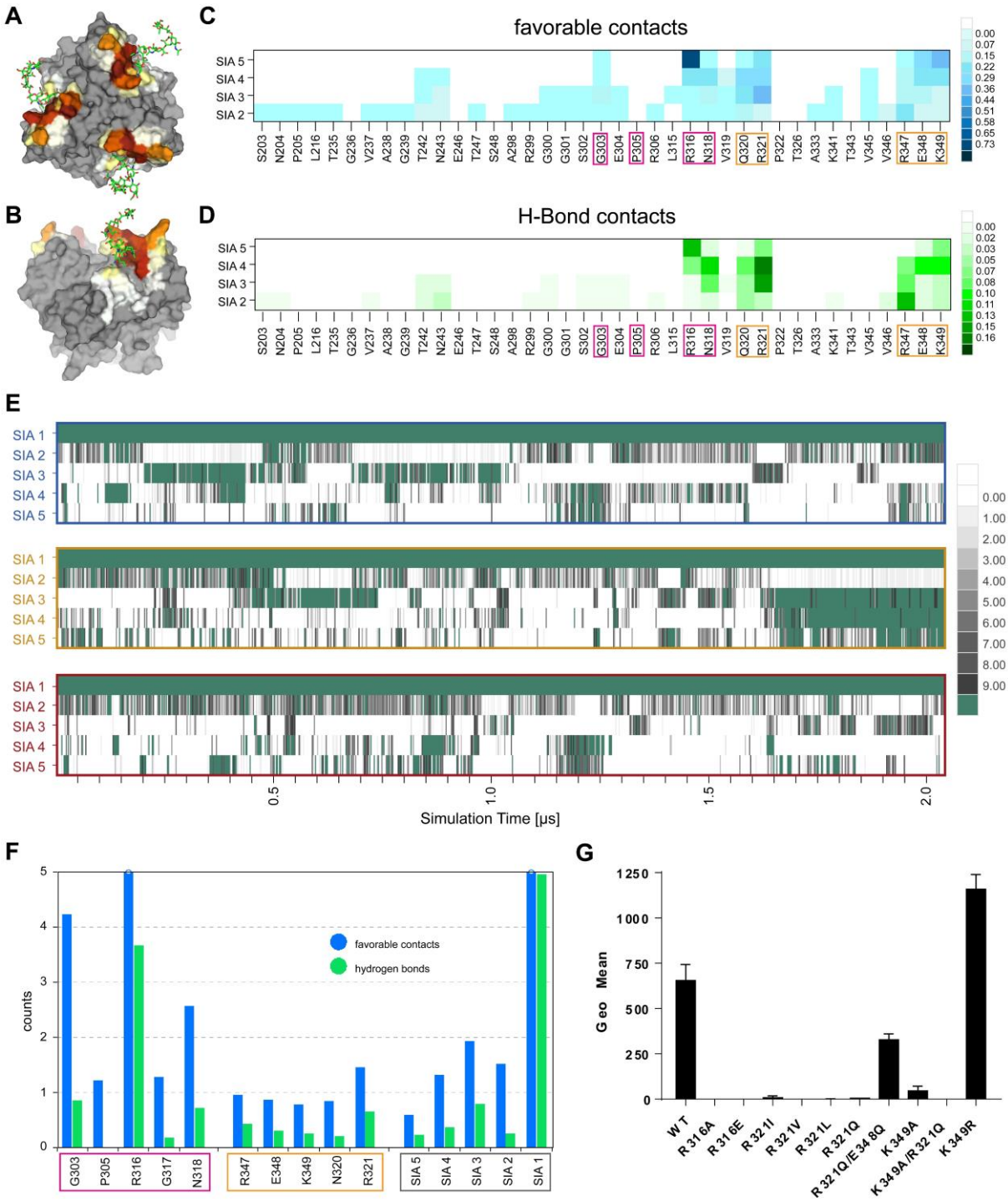

Fig. 7. Molecular dynamics simulation of the interactions between 52SFK and DP5. Three pentasialic acid (DP5) molecules interacting with the three identical binding pockets of 52SFK were simulated over a time of 2 µs. (A-B) The interaction profile of DP5 with the protein is mapped onto 52SFK in a 'heat map' style. Non-interacting residues are colored in

gray, interacting residues are scored from white (few interactions) to brown (strongly interacting). (A) All three pockets are shown from a top view. (B) One of the simulated binding pockets is shown from a side view. (C-D) Detailed interactions contributed by the additional sialic acid moieties in polySia. Amino acids of the canonical binding site are boxed in pink, residues of the 'steering rim' in orange. (C) Residue-residue interaction matrix showing the average number of favorable atom contacts between individual amino acids and sialic acids (SIA 2-5, counted from the non-reducing end) over the whole simulation. (D) Analogous plot showing the average number of hydrogen bonds. (E) Time-resolved trajectory plot of the number of atom contacts per sialic acid residue (numbered from the non-reducing end) in the three binding sites (individual rows) averaged over 2.5 ns increments. Atom contacts are counted as favorable if one of the following conditions are satisfied: H-bond donor/acceptor atom distance < 3.2 Å or C-C atom distance < 4.2 Å. The average number of interactions is depicted according to the color legends on the right for each panel. (F) Summary of the interactions of polySia with the 52SFK canonical pocket and 'steering rim'. The number of favorable atom contacts and hydrogen bonds per residue is averaged over the three binding sites. Boxing of the amino acid residues is analogous to panels C & D, sialic acids are boxed in grey. (G) Flow cytometry-based analysis of HAdV-52 short fiber knob mutant binding to polysialic acid-expressing SH-SY5Y cells. The experiment was performed three times with duplicate samples in each experiment. Error bars represent mean ± SD.

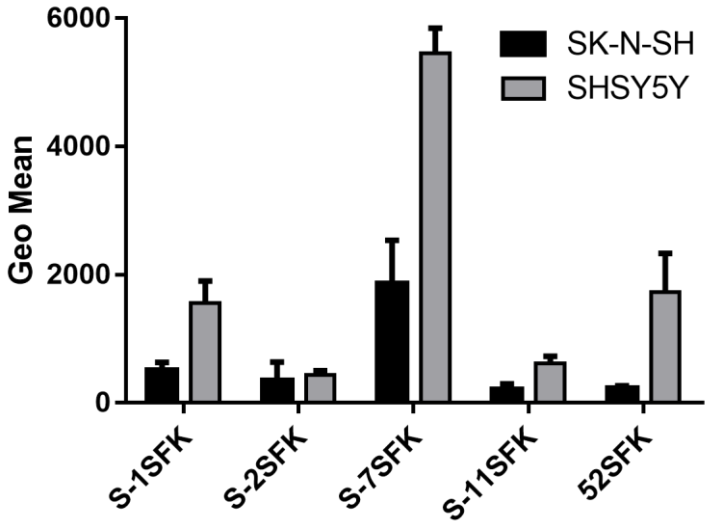

Fig. 8. AdV short fiber knob binding to polysialic acid-expressing/-lacking cells. Flow cytometry-based quantification of simian (S) and human AdV short fiber knob binding to human neuroblastoma cells expressing (SH-SY5Y) or lacking (SK-N-SH) polySia. The experiment was performed three times with duplicate samples in each experiment. SFK: short fiber knob; FK: fiber knob. Error bars represent mean ± SD.

SUPPORTING INFORMATION

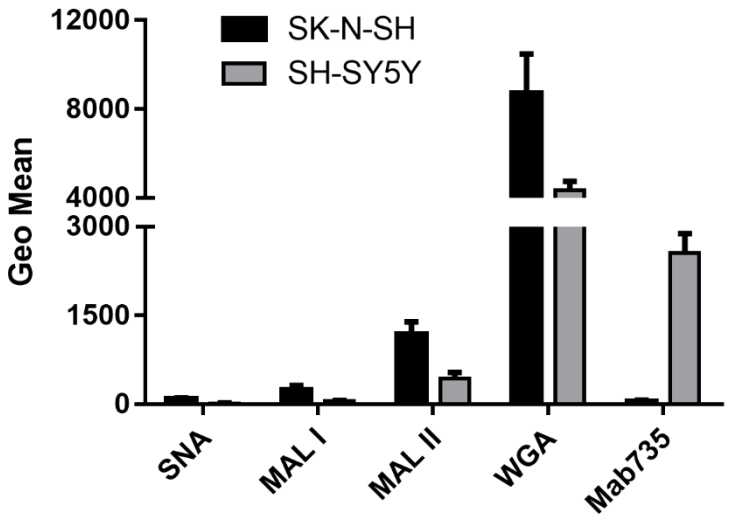

Fig. S1. Relative expression levels of sialic acid-containing glycans on SK-N-SH and SH-SY5Y cells. Sialic acid expression was determined using the sialic acid-binding lectins Sambucus Nigra (SNA, binds to α2,6-linked sialic acid), Maackia Amurensis I and II (MAL I & MAL II, both binds to α2,3-linked sialic acid) and wheat germ agglutinin (WGA binds to terminal sialic acid as well as to N-acetyl-D-glucosamine). PolySia expression was determined using an anti-polySia antibody (mab735). The experiment was performed three times with duplicate samples in each experiment. Error bars represent mean ± SD.

A

	ϕ C1-C2-O-C8	ψ C2-O-C8-C7	ω C9-C8-C7-C6	χ C8-C7-C6-C5
DP3	-55,45	121,38	69,79	168,74
DP4	-41,90	116,76	46,26	164,96
DP5	-45,33	128,74	40,84	165,53

B

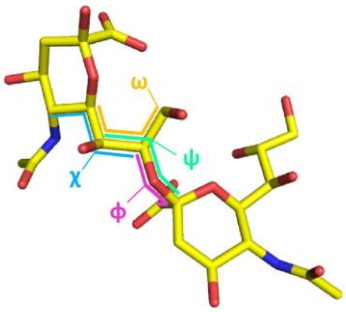

Fig. S2. Observed glycosidic angles in 52SFK / polySia complex structures. (A) Torsion angles observed for polySia of different DP in the complex crystal structures. All angles adopt similar conformations. (B) Definition of the glycan torsion angles as in (83).

A

```
HAdV-52      IQTLWTPPTSNPNCTVYTESDSLLSLCLTKCGAHVLGSVSLTGVAGTMTNMA-ETSLAIE
SAdV-1       IQTLWTAPTSTGNCTVYSEGDSLLSLCLTKCGAHVLGSVSLTGLTGTITQMT-DISVTIQ
SAdV-2       SQTLWTNPNETANCSVFQSLDSLLTLCLTKNGAHVLGSVSLTGLSGPLLKMT-TTSVTVQ
SAdV-7       IQSLWTFPTKTPNCTVFTESDSLLSLCLTKCGAHVLGSVSLSGVAGTMLKMT-HTSVTVQ
SAdV-11      IQSLCTTPTAASNCTVFTNGDSLLCLCLTKCGAHVLGSVSLTGMQGTITAMT-QNYISIQ
SAdV-19      PISLWTQPTTTANCTVYQTLDSQFLLCLTKNDAHIVGSVCLTGLQGTLNNLPTNTTVTVE
HAdV-41      LTTIWSI-SPTPNCSIYETQDANLFLCLTKNGAHVLGTITIKGLKGALREMH-DNALSLK
HAdV-40      LTTIWSI-SPTPNCSIYETQDANLFLCLTKNGAHVLGTITIKGLKGALREMN-DNALSVK
               :: :  .   **:::   *: : ***** .**::*:: :.*: * :  :     ::::

HAdV-52      FTFDDTGKLLHSPLVN-NTFSIRQGDSPASNPTYNALAFMPNSTLYARGGSGEPRNNYYV
SAdV-1       FTFDNNGKLLSSPLIN-NAFSIRQNDSTASNPTYNALAFMPNSTIYARGGGGEPRNNYYV
SAdV-2       LIFDSNGVLTTSQLNT-NSWGMRA-NTNLNAPVTNALPFMPNSTIYARGNAGEPRSNYYV
SAdV-7       FSFDDSGKLIFSPLAN-NTWGVRQSESPLPNPSFNALTFMPNSTIYSRGASNEPQNNYYV
SAdV-11      FLFDHNGALTSSPLLNNNTWGIRQSDTSSANPAYNALAFMPNSTVYVRGQSGEPRNNYYT
SAdV-19      LIFNSDGQLQSSPLVA-DSWGIREQNAS--TEVSNAIQFMPNSLIYTRGQAGDPKNNYYT
HAdV-41      LPFDNQGNLLNCALES-STWRYQETNAV----ASNALTFMPNSTVYPRNKTAHPGNMLI-
HAdV-40      LPFDNQGNLLNCALES-STWRYQETNAV----ASNALTFMPNSTVYPRNKTADPGNMLI-
             : *:  * *  . *   .::  :  ::       **: ***** :* *.   .* .

HAdV-52      QTYLRGNVQRPITLTVTFNSAA-----TGYSLSFKWT-AVVREKFAAPATSFCYITEQ
SAdV-1       QTYLRGNVQKPIILTVTYNSVA-----TGYSLSFKWT-ALAREKFATPTTSFCYITEQ
SAdV-2       QTYLRGNLNKQITLSISFNASS-----SGYSLTFKWS-AIATEKFATPTSSFCYIAEQ
SAdV-7       QTYLRGNVRKPILLTVTYNSVN-----SGYSLTFKWD-AVANEKFATPTSSFCYVAEQ
SAdV-11      QTYLRGNVKKPIILTVTYNSAA-----SGYSLTFKWD-AVVTEKFATPTSSFCYITEQ
SAdV-19      TTYLRGNTGRPIILTVTLNGSSSIASTNQYSLTFRWRNTYANERFSTPFASFVYIAEQ
HAdV-41      ------QISPNITFSVVYNEIN-----SGYAFTFKWS-AEPGKPFHPPTAVFCYITEQ
HAdV-40      ------QISPNITFSVVYNEIN-----SGYAFTFKWS-AEPGKPFHPPTAVFCYITEQ
                   :    * :::  *        . *:::*:*  :   : *  * : * *::**
```

B

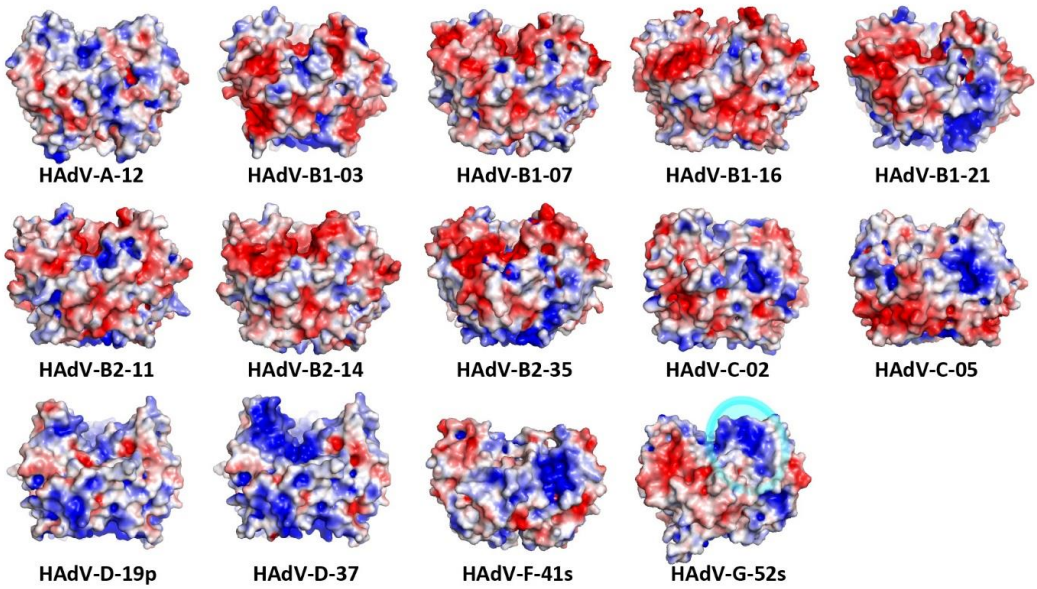

C

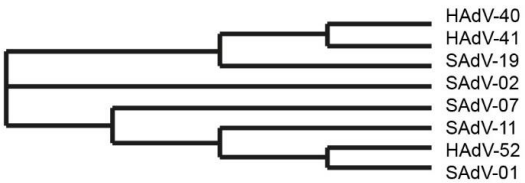

Fig. S3. AdV fiber knobs and polysialic acid. (A) Sequence alignment of AdV knobs closely related to HAdV-52. Residues of the 'steering rim' and their functional analogues are highlighted in cyan, the additional residues of the RGN motif in yellow, and the negatively charged E348 in orange. Sequences are ordered by name. (B) Poisson-Boltzmann electrostatic surface potentials of known HAdV fiber knobs across all species. Electrostatic surface potentials have been calculated at ±3 kT/e, electropositive batches are displayed in blue. (C) Phylogenetic cladogram of the short fiber knob sequences based on ClustalOmega alignment.

Movie S1. Molecular dynamics simulation of the complex between 52SFK and pentasialic acid (DP5).

Table S1. List of sialylated glycans included in the microarray screening analysis.

Position	Probe[a]	Sequence	Fluorescence Intensity[b,c]	Error[d]
1	Lac-AO	Galβ-4Glc-AO	27	13
2	LacNAc-AO	Galβ-4GlcNAc-AO	-	93
3	LNT	Galβ-3GlcNAcβ-3Galβ-4Glc-DH	10	79
4	LNnT	Galβ-4GlcNAcβ-3Galβ-4Glc-DH	430	18
5	LNFP-III	Galβ-4GlcNAcβ-3Galβ-4Glc-DH | Fucα-3	154	224
6	NA2	Galβ-4GlcNAcβ-2Manα-6 | Manβ-4GlcNAcβ-4GlcNAc-DH | Galβ-4GlcNAcβ-2Manα-3	113	188
7	GM4	NeuAcα-3Galβ-Cer	-	113
8	GM3	NeuAcα-3Galβ-4Glcβ-Cer	-	106
9	GM3(Gc)	NeuGcα-3Galβ-4Glcβ-Cer	-	191
10	Haematoside	NeuAcα-3Galβ-4Glcβ-Cer	-	36
11	NeuAcα-(3')Lac-AO	NeuAcα-3Galβ-4Glc-AO	755	19
12	GSC-199	KDNα-3Galβ-4Glcβ-C30	-	71
13	NeuAcβ-(3')Lac-AO	NeuAcβ-3Galβ-4Glc-AO	832	52
14	Neuα-(3')Lac-AO	Neuα-3Galβ-4Glc-AO	667	118
15	Neu4,5Ac-(3')Lac-AO	(4-OAc)NeuAcα-3Galβ-4Glc-AO	750	339
16	GSC-75	(4-deoxy)NeuAcα-3Galβ-4Glcβ-Cer36	221	215
17	GSC-76	(7-deoxy)NeuAcα-3Galβ-4Glcβ-Cer36	-	182
18	GSC-77	(8-deoxy)NeuAcα-3Galβ-4Glcβ-Cer36	-	32
19	GSC-51	(9-deoxy)NeuAcα-3Galβ-4Glcβ-Cer36	-	84
20	GSC-78	(4-OMe)NeuAcα-3Galβ-4Glcβ-Cer36	84	53
21	GSC-79	(9-OMe)NeuAcα-3Galβ-4Glcβ-Cer36	-	20
22	GSC-161	NeuAcα-3Galβ-4Glcβ-C30 | Fucα-3	-	195
23	NeuAcα-(3')LN1-3-AO	NeuAcα-3Galβ-3GlcNAc-AO	266	21

24	NeuAcα-(3')LN	NeuAcα-3Galβ-4GlcNAc-DH	326	13
25	NeuAcα-(3')LN-AO	NeuAcα-3Galβ-4GlcNAc-AO	55	103
26	SA(3')-Lea-Tri-AO	NeuAcα-3Galβ-3GlcNAc-AO | Fucα-4	2	103
27	SA(3')-Lex-Tri-AO	NeuAcα-3Galβ-4GlcNAc-AO | Fucα-3	308	106
28	GSC-440	NeuAcα-3Galβ-4GlcNAcβ-C30 | Fucα-3	11	77
29	GSC-512	(4-OAc)NeuAcα-3Galβ-4GlcNAcβ-C30 | Fucα-3	-	96
30	GSC-513	(9-OAc)NeuAcα-3Galβ-3GlcNAcβ-C30 | Fucα-4	-	124
31	GSC-511	(9-OAc)NeuAcα-3Galβ-4GlcNAcβ-C30 | Fucα-3	-	108
32	GSC-479	NeuAcα-3Galβ-4GlcNAcβ-3Galβ-C30 | Fucα-3	577	287
33	GSC-105	NeuAcα-3Galβ-4GlcNAcβ-3Galβ-Cer36 | Fucα-3	-	26
34	GSC-177	NeuGcα-3Galβ-4GlcNAcβ-3Galβ-Cer36 | Fucα-3	129	67
35	GSC-341	KDNα-3Galβ-4GlcNAcβ-3Galβ-C30 | Fucα-3	-	342
36	GSC-257	NeuAcα-3(4,6-deoxy)Galβ-4GlcNAcβ-3Galβ-Cer36 | Fucα-3	201	114
37	GSC-175	NeuAcα-3(4-deoxy)Galβ-4GlcNAcβ-3Galβ-Cer36 | Fucα-3	-	296
38	GSC-176	NeuAcα-3(6-deoxy)Galβ-4GlcNAcβ-3Galβ-Cer36 | Fucα-3	326	3
39	LSTa	NeuAcα-3Galβ-3GlcNAcβ-3Galβ-4Glc-DH	108	101
40	GSC-272	NeuAcα-3Galβ-3GlcNAcβ-3Galβ-4Glcβ-C30	-	88
41	GSC-273	NeuAcα-3Galβ-4GlcNAcβ-3Galβ-4Glcβ-C30	8436	1162
42	GSC-396	NeuGcα-3Galβ-3GlcNAcβ-3Galβ-4Glcβ-C30	106	184
43	Sialylparagloboside	NeuAcα-3Galβ-4GlcNAcβ-3Galβ-4Glcβ-Cer	-	53
44	GSC-31	NeuAcα-3Galβ-4GlcNAcβ-3Galβ-4Glcβ-Cer36	79	53
45	GSC-516B	Neuα-3Galβ-4GlcNAcβ-3Galβ-4Glcβ-Cer36 | SU-6	-	178
46	C4U	NeuAcα-3Galβ-4GlcNAcβ-3Galβ-3GlcNAc-DH | | | SU-6 SU-6 SU-6	2732	655
47	SA(3')-LNFP-II	NeuAcα-3Galβ-3GlcNAcβ-3Galβ-4Glc-DH | Fucα-4	396	148
48	SA(3')-LNFP-III	NeuAcα-3Galβ-4GlcNAcβ-3Galβ-4Glc-DH | Fucα-3	175	128
49	GSC-64	NeuAcα-3Galβ-4GlcNAcβ-3Galβ-4Glcβ-Cer36 | Fucα-3	-	167
50	GSC-533	NeuAcα-3Galβ-4GlcNβ-3Galβ-4Glcβ-Cer36 | Fucα-3	-	162
51	GSC-149	KDNα-3Galβ-4GlcNAcβ-3Galβ-4Glcβ-Cer36 | Fucα-3	-	54
52	GSC-472	Neuα-3Galβ-4GlcNAcβ-3Galβ-4Glcβ-Cer36 | Fucα-3	-	58
53	GSC-268	SU-6 | NeuAcα-3Galβ-4GlcNAcβ-3Galβ-4Glcβ-Cer36 | Fucα-3	1392	63
54	GSC-268 deNAc	SU-6 | Neuα-3Galβ-4GlcNβ-3Galβ-4Glcβ-Cer36 | Fucα-3	249	168
55	GSC-269	SU-6 | NeuAcα-3Galβ-4GlcNAcβ-3Galβ-4Glcβ-Cer36 | Fucα-3	447	98
56	GSC-406	SU-6 | Neuα-3Galβ-4GlcNAcβ-3Galβ-4Glcβ-Cer36 | Fucα-3	419	57

57	GSC-270	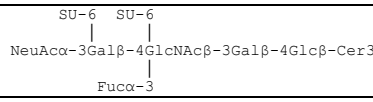	3219	125
58	GSC-220	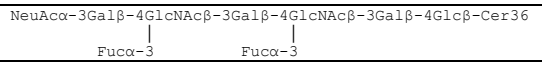	24	257
59	GSC-221	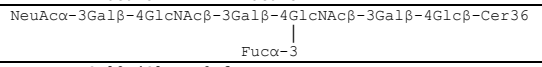	527	18
60	MSMFLNH	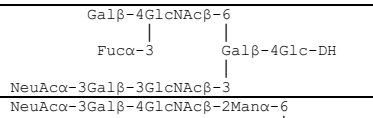	1	22
61	A2F(2-3)	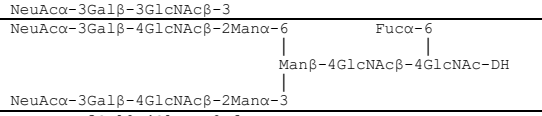	3575	256
62	P22-1 (GTP 3N(2,3)-3A(2,6)+F)	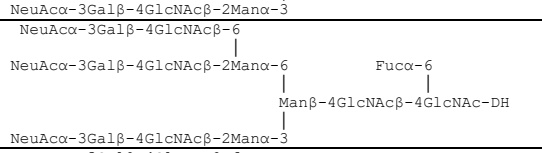	211	15
63	P6-1 (GTP 4N(2,3)-4A+F)	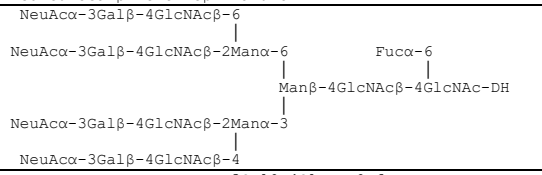	139	115
64	P7-2 (GTP 4N(2,3)-4A+1R+F)	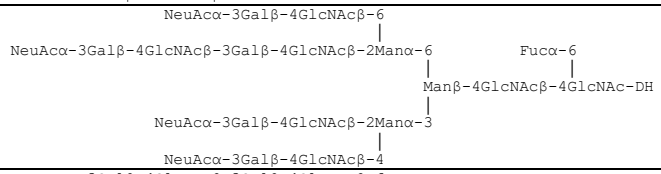	137	137
65	P8-1 (GTP 4N(2,3)-4A+2R+F)	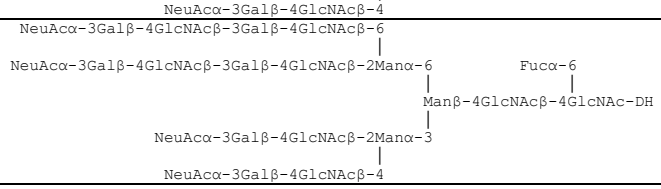	185	216
66	GM2	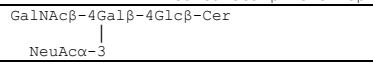	-	507
67	GM1	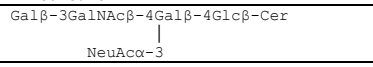	-	167
68	GM1-penta	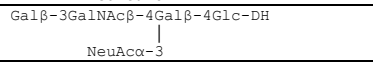	-	18
69	GM1(Gc)	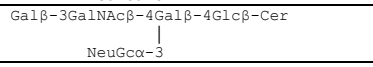	-	93
70	GM1(Gc)-penta	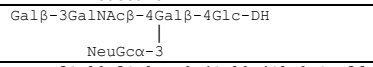	-	103
71	GSC-195	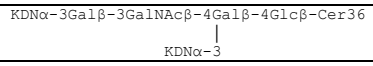	107	127
72	GD1a	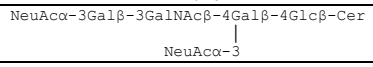	-	107
73	GD1a-hexa	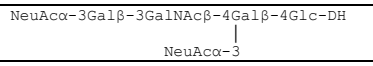	2356	223
74	GSC-335	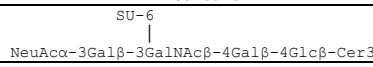	547	398
75	GSC-488	NeuAcα-3Galβ-3GalNAcβ-C30	50	50
76	GSC-489	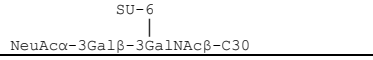	963	7
77	GSC-154	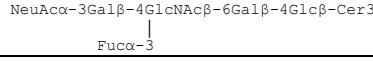	-	368
78	GSC-441	NeuAcα-3Galβ-4GlcNAcβ-6GalNAcα-3Galβ-4Glcβ-C30	1193	271
79	GSC-384	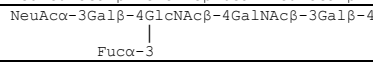	478	29
80	GSC-284	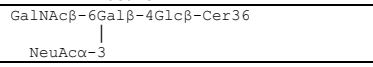	531	222
81	GSC-27	NeuAcα-6Galβ-Cer36	39	183
82	GSC-61	NeuAcα-6Galβ-4Glcβ-Cer36	-	156

83	NeuAcα-(6')Lac-AO	NeuAcα-6Galβ-4Glc-AO	335	321
84	NeuAcβ-(6')Lac-AO	NeuAcβ-6Galβ-4Glc-AO	476	92
85	Neuα-(6')Lac-AO	Neuα-6Galβ-4Glc-AO	390	500
86	NeuAcα-(6')LN	NeuAcα-6Galβ-4GlcNAc-DH	-	90
87	NeuAcα-(6')LN-AO	NeuAcα-6Galβ-4GlcNAc-AO	-	259
88	Neu5,9Ac-(6')LN	(9-OAc)NeuAcα-6Galβ-4GlcNAc-DH	-	159
89	LSTb	Galβ-3GlcNAcβ-3Galβ-4Glc-DH | NeuAcα-6	1243	22
90	LSTc	NeuAcα-6Galβ-4GlcNAcβ-3Galβ-4Glc-DH	-	235
91	GSC-397	NeuGcα-6Galβ-3GlcNAcβ-3Galβ-4Glcβ-C30	-	386
92	GSC-97	NeuAcα-6Galβ-4GlcNAcβ-3Galβ-4Glcβ-Cer36 | Fucα-3	-	55
93	SA(6')-LNFP-VI	NeuAcα-6Galβ-4GlcNAcβ-3Galβ-4Glc-DH | Fucα-3	-	32
94	MSLNH	NeuAcα-6Galβ-4GlcNAcβ-6 | Galβ-4Glc-DH | Galβ-3GlcNAcβ-3	-	229
95	MSLNnH-I	Galβ-4GlcNAcβ-6 | Galβ-4Glc-DH | NeuAcα-6Galβ-3GlcNAcβ-3	138	41
96	DSLNnH	NeuAcα-6Galβ-4GlcNAcβ-6 | Galβ-4Glc-DH | NeuAcα-6Galβ-4GlcNAcβ-3	-	145
97	MFMSLNnH	Galβ-4GlcNAcβ-6 | Fucα-3 Galβ-4Glc-DH | NeuAcα-6Galβ-3GlcNAcβ-3	-	23
98	A2(2-6)	NeuAcα-6Galβ-4GlcNAcβ-2Manα-6 | Manβ-4GlcNAcβ-4GlcNAc-DH | NeuAcα-6Galβ-4GlcNAcβ-2Manα-3	66	291
99	AGP-Bi-Ac2	NeuAcα-6Galβ-4GlcNAcβ-2Manα-6 | Manβ-4GlcNAcβ-4GlcNAc-DH | NeuAcα-6Galβ-4GlcNAcβ-2Manα-3	700	166
100	AGP-Bi-Gc2	NeuGcα-6Galβ-4GlcNAcβ-2Manα-6 | Manβ-4GlcNAcβ-4GlcNAc-DH | NeuGcα-6Galβ-4GlcNAcβ-2Manα-3	1222	221
101	GSC-442	GalNAcβ-4Galβ-4Glcβ-Cer36 | NeuAcα-6	70	147
102	GSC-68	NeuAcα-6Galβ-3GalNAcβ-4Galβ-4Glcβ-Cer36	652	155
103	GSC-155	Galβ-3GalNAcβ-4Galβ-4Glcβ-Cer36 | NeuAcα-6	444	59
104	GSC-107	NeuAcα-6Galβ-3GalNAcβ-4Galβ-4Glcβ-Cer36 | NeuAcα-6	704	32
105	GSC-70	NeuAcα-6Galβ-6GalNAcβ-4Galβ-4Glcβ-Cer36	174	70
106	DST	NeuAcα-3Galβ-3GalNAc-DH | NeuAcα-6	1086	122
107	DST-AO	NeuAcα-3Galβ-3GalNAc-AO | NeuAcα-6	3027	163
108	GSC-490	NeuAcα-3Galβ-3GalNAcβ-C30 | NeuAcα-6	-	74
109	DSLNT	NeuAcα-3Galβ-3GlcNAcβ-3Galβ-4Glc-DH | NeuAcα-6	3213	147
110	A3	NeuAcα-3Galβ-4GlcNAcβ-2Manα-6 | Manβ-4GlcNAcβ-4GlcNAc-DH | NeuAcα-3Galβ-4GlcNAcβ-4Manα-3 | NeuAcα-6Galβ-4GlcNAcβ-2	3473	391
111	GSC-118	NeuAcα-3Galβ-3GalNAcβ-4Galβ-4Glcβ-Cer36 | NeuAcα-6	195	198
112	GSC-230	NeuAcα-8NeuAcα-3Galβ-Cer36	223	93
113	GSC-231	NeuAcα-8NeuAcα-6Galβ-Cer36	58	122
114	GSC-439	NeuAcα-8NeuAcα-8NeuAcα-6Galβ-Cer36	454	122
115	GD3	NeuAcα-8NeuAcα-3Galβ-4Glcβ-Cer	391	77
116	GD3-tetra-AO	NeuAcα-8NeuAcα-3Galβ-4Glc-AO	873	5
117	GSC-229	NeuAcα-8NeuAcα-3Galβ-4Glcβ-Cer36	319	18

118	GSC-437	NeuAcα-8NeuAcα-8NeuAcα-3Galβ-4Glcβ-Cer36	-	191
119	GD2	GalNAcβ-4Galβ-4Glcβ-Cer | NeuAcα-8NeuAcα-3	228	14
120	GD1b	Galβ-3GalNAcβ-4Galβ-4Glcβ-Cer | NeuAcα-8NeuAcα-3	800	74
121	GQ1b	NeuAcα-8NeuAcα-3Galβ-3GalNAcβ-4Galβ-4Glcβ-Cer | NeuAcα-8NeuAcα-3	673	47
122	SA3(α8)	NeuAcα-8NeuAcα-8NeuAc-DH	4026	303
123	SA5(α8)*	NeuAcα-8NeuAcα-8NeuAcα-8NeuAcα-8NeuAc-DH	31735	167
124	SA7(α8)*	NeuAcα-8NeuAcα-8NeuAcα-8NeuAcα-8NeuAcα-8NeuAcα-8NeuAc-DH	28224	86
125	SA9(α8)*	NeuAcα-8NeuAcα-8NeuAcα-8NeuAcα-8NeuAcα-8NeuAc-8NeuAcα-8NeuAc-8NeuAcα-DH	32320	954
126	GT1a	NeuAcα-8NeuAcα-3Galβ-3GalNAcβ-4Galβ-4Glcβ-Cer | NeuAcα-3	781	272
127	GT1b	NeuAcα-3Galβ-3GalNAcβ-4Galβ-4Glcβ-Cer | NeuAcα-8NeuAcα-3	2104	79
128	GSC-96	NeuAcα-9NeuAcα-3Galβ-4Glcβ-Cer36	-	152

[a] The glycan probes are all lipid-linked, neoglycolipids (NGLs) or glycosylceramides and are from the collection assembled in the course of research in the Glycosciences Laboratory. For definition of the lipid moieties of the probes, please see https://glycosciences.med.ic.ac.uk/docs/lipids.pdf.

[b] Numerical scores for the binding signals are shown as means of duplicate spots at 5 fmol per spot.

[c] -, signal less than 1.

[d] Difference of signal intensities of duplicated spots of each glycan probe.

Table S2. Supplementary Glycan Microarray Document based on MIRAGE guidelines (doi:10.3762/mirage.3)

Classification	Guidelines
1. Sample: Glycan Binding Sample	
Description of Sample	Sample name: HAdV-52 fiber-1 or HAdV52 SFK (abbreviated as 52SFK in the main text) Previous reference: Lenman et al. PLoS pathogens (2015). PMID: 25674795. Public database IDs: DQ923122.2 in the Genbank https://www.ncbi.nlm.nih.gov/nuccore/124375632/ ABK35058.1 in the Protein sequence database https://www.ncbi.nlm.nih.gov/protein/ABK35058.1 4XL8 in PDB as well as the PDB entry of the construct used in this publication (ID 4XL8). http://www.rcsb.org/pdb/explore/explore.do?structureId=4XL8 Origin: recombinant. Method of preparation: DNA fragment encoding the knob domain of the short fiber (SFK) was isolated from virions of Species G HAdV-52 (strain TB3-2243) and cloned into a pQE30Xa expression vector encoding an N-terminal His-tag. The protein HAdV52 SFK was expressed in Escherichia coli (strain M15) and purified with Ni-NTA agarose beads. Proteins were analyzed by denaturing gel (NuPAGE Bis-Tris, Invitrogen, Life Technologies) and western blot with monoclonal antibodies directed against the His-tag (Qiagen).
Sample modifications	Not relevant.
Assay protocol	Please see method section in the main text.
2. Glycan Library	
Glycan description for defined glycans	The microarray (in house designation 'Sialyl Glycan Array Sets 40,41') contained 128 lipid-linked glycan probes, neoglycolipids (NGLs) or glycosylceramides, which are from the collection assembled in the course of research in the Glycosciences Laboratory (https://glycosciences.med.ic.ac.uk/glycanLibraryList.html). The probe names and structures are in **Supplementary Table S3**.
Glycan description for undefined glycans	Not relevant.

Glycan modifications	Unless otherwise specified the NGLs were prepared from reducing oligosaccharides by reductive amination with the amino lipid, 1,2-dihexadecyl-sn-glycero-3-phosphoethanolamine [(DHPE) (Chai et al., Methods Enzymol. 2003)]; AO, NGLs prepared from reducing oligosaccharides by oxime ligation with an aminooxy functionalized DHPE [(AOPE) (Liu et al., Chem. Biol. 2007)]. For full description on the definition of the lipid moieties of the glycan probes, please see https://glycosciences.med.ic.ac.uk/docs/lipids.pdf.
3. Printing Surface; e.g., Microarray Slide	
Description of surface	Nitrocellulose-coated glass microarray slides.
Manufacturer	Whatman® FAST 16-pad Slides
Custom preparation of surface	Not relevant.
Non-covalent Immobilization	The lipid-linked glycan probes were formulated as liposomes by adding carrier lipids, phosphatidylcholine and cholesterol (Liu et al., Methods Mol. Biol. 2012) for robotically arraying and non-covalent immobilization on nitrocellulose-coated glass slides.
4. Arrayer (Printer)	
Description of Arrayer	Piezorray (PerkinElmer LAS, Beaconsfield, UK)
Dispensing mechanism	Non-contact liquid delivery with four dispensing tips.
Glycan deposition	Approximate 0.33 nl was printed for each spot. Each glycan probe was printed at two levels (2 and 5 fmol per spot) in duplicate.
Printing conditions	The printing solutions contained 100 pmol/µl of phosphatidylcholine and cholesterol (both from SIGMA) as lipid carriers in addition to the lipid-linked glycan probes in water (HPLC grade). The concentrations of the lipid-linked glycan probes were 5 and 15 pmol/µl for the 2 and 5 fmol per spot levels, respectively. The printing solutions also contained Cy3 NHS ester (GE Healthcare) at 20 ng/ml (26 fmol/µl) as a marker to monitor the printing process.
5. Glycan Microarray with "Map"	
Array layout	Each array slide contained 16-pad subarrays. Each subarray contained 64 glycan probes printed at two levels in duplicate (four spots for one probe in a row); 256 spots (16x16) in total for 64 probes. There are 128 glycan probes (in 2 subarrays) present in the arrays of 'Sialyl Glycan Array Sets 40,41'.
Glycan identification and quality control	The 128 glycan probes printed are defined in **Supplementary Table S3**. The quality control of the glycan probes on the arrays was carried out by analyses with biotinylated plant lectins including wheat germ agglutinin (WGA), *Sambucus nigra* lectin (SNL) and *Maackia*

	amurensis Lectin I (MAL I) (Vector Labs) as well as a number of influenza viruses (Crusat et al, Virology. 2013). These data are not included in the present paper but available on request.
6. Detector and Data Processing	
Scanning hardware	ProScanArray microarray scanner (PerkinElmer LAS, Beaconsfield, UK)
Scanner settings	Scanning resolution: 10 μm / pixel (this resolution is adequate for the sizes of sample spots) Laser channel: Red (scan wavelength 633 nm) PMT Voltages: 35 Scan power: 85%
Image analysis software	ScanArray Express software (PerkinElmer LAS, Beaconsfield, UK).
Data processing	The gpr file was entered into an in-house microarray database using software (designed by Dr Mark Stoll, http://www.beilstein-institut.de/en/publications/proceedings/glyco-2009) for data processing. No particular normalization method or statistical analysis was used.
7. Glycan Microarray Data Presentation	
Data presentation	The microarray binding results are in **Figure 1** and **Supplementary Table S3**. The table includes the list of glycan probes present in the array, binding intensities at the 5 fmol per spot level and errors (difference of signal intensities of duplicate spots of each glycan probe).
8. Interpretation and Conclusion from Microarray Data	
Data interpretation	No software or algorithms were used to interpret processed data.
Conclusions	52SFK bound strongly to [α-2,8]-linked (poly) sialic acid sequences (DP>3), and weakly to a number of α2,3-sialylated probes.

Table S3. Data collection statistics of 52SFK complex structures.

	GD3	PSia DP3	PSia DP4	Psia DP5
Beamline	X06DA (PXIII)	X06DA (PXIII)	X06DA (PXIII)	X06DA (PXIII)
Detector	Pilatus 2M	Pilatus 2M	Pilatus 2M	Pilatus 2M
Angle increment [°]	0.1	0.1	0.1	0.1
Total rotation angle [°]	360	360	360	360
Wavelength [Å]	1.00	1.00	0.92	0.92
Data collection				
Resolution [Å]	50.0 - 1.17 (1.25 - 1.17)	50 - 1.50 (1.59 - 1.50)	50 - 1.35 (1.43 - 1.35)	50 - 1.48 (1.57 - 1.48)
Completeness [%]	99.0 (88.0)	97.7 (94.7)	99.5 (97.0)	99.5 (97.1)
Observed	2,103,614 (289,758)	1,041,202 (150,022)	1,412,870 (216,260)	1,078,654 (154,372)
Redundancy	13.3 (12.3)	13.2 (12.3)	13.1 (12.9)	13.1 (12.1)
CC1/2* [%]	100.0 (75.3)	100.0 (66.8)	100.0 (72.3)	100.0 (70.1)
I/σI	22.7 (2.4)	21.3 (2.0)	23.6 (2.2)	23.5 (2.2)
Wilson B-Factor [Å^2]	17.0	16.9	14.8	15.8
FreeR [% of reflections]	5	5	5	5
Crystal properties				
Space group	$P2_12_12_1$	$P2_12_12_1$	$P2_12_12_1$	$P2_12_12_1$
Unit cell axes [Å]	a=63.88	a=64.80	a=63.89	a=63.92
	b=82.03	b=81.80	b=93.16	b=81.70
	c=93.31	c=93.40	c=81.77	c=93.39
Unit cell angles [°]	α=β=γ=90	α=β=γ=90	α=β=γ=90	α=β=γ=90

Table S4. Refinement statistics of 52SFK complex structures.

		GD3	PSia DP3	PSia DP4	Psia DP5
Rwork [%]		11.95	16.56	16.65	15.06
Rfree [%]		14.06	18.25	18.81	17.76
Rmsd bond [Å]		0.016	0.009	0.011	0.015
Rmsd angles [°]		1.729	1.353	1.426	1.624
B-Factor [Å^2]	overall	16.87	20.8	17.8	21.2
	protein	15.47	19.9	18.8	17.8
	solvent	29.80	26.0	24.6	30.3
	ligand	25.31	38.3	31.4	34.8
No of atoms					
protein		4077	3811	3817	3927
ligand		21	41	41	40
solvent		511	237	263	324
Ramachandran favored (%)		98.1	98.1	98.1	97.7
Ramachandran allowed (%)		1.9	1.9	1.9	2.1
Ramachandran outliers (%)		0	0	0	0.2